International Journal of Nanomedicine

Dovepress
open access to scientific and medical research

Open Access Full Text Article

ORIGINAL RESEARCH

Nanocurcumin Reduces High Glucose and Particulate Matter-Induced Endothelial Inflammation: Mitochondrial Function and Involvement of miR-221/222

Tsai-Chun Lai[1–3], Chiang-Wen Lee[4–6], Mei-Hsiang Hsu[1], Yu-Chen Chen[1,7], Shu-Rung Lin[8,9], Shu-Wha Lin[10], Tzu-Lin Lee[1], Shin-Yu Lin[11,12], Shu-Hao Hsu[1], Jaw-Shiun Tsai[13,14], Yuh-Lien Chen[1]

[1]Department of Anatomy and Cell Biology, College of Medicine, National Taiwan University, Taipei, Taiwan, Republic of China; [2]Department of Life Sciences, College of Life Sciences, National Chung Hsing University, Taichung, Taiwan, Republic of China; [3]The iEGG and Animal Biotechnology Center, National Chung Hsing University, Taichung, Taiwan, Republic of China; [4]Department of Orthopaedic Surgery, Chang Gung Memorial Hospital, Puzi City, Chiayi County, Taiwan, Republic of China; [5]Department of Nursing, Division of Basic Medical Sciences, and Chronic Diseases and Health Promotion Research Center, Chang Gung University of Science and Technology, Puzi City, Chiayi County, Taiwan, Republic of China; [6]Research Center for Industry of Human Ecology and Research Center for Chinese Herbal Medicine, Chang Gung University of Science and Technology, Taoyuan City, Taiwan, Republic of China; [7]Department of Medicine, Mackay Medical College, New Taipei City, Taiwan, Republic of China; [8]Department of Bioscience Technology, College of Science, Chung-Yuan Christian University, Taoyuan, Taiwan, Republic of China; [9]Center for Nanotechnology and Center for Biomedical Technology, Chung-Yuan Christian University, Taoyuan, Taiwan, Republic of China; [10]Department of Clinical Laboratory Sciences and Medical Biotechnology, College of Medicine, National Taiwan University, Taipei, Taiwan, Republic of China; [11]Department of Obstetrics and Gynecology, National Taiwan University Hospital, Taipei, Taiwan; [12]Department of Obstetrics and Gynecology, National Taiwan University College of Medicine, Taipei, Taiwan, Republic of China; [13]Department of Family Medicine, National Taiwan University Hospital, Taipei, Taiwan, Republic of China; [14]Center for Complementary and Integrated Medicine, National Taiwan University Hospital, Taipei, Taiwan, Republic of China

Correspondence: Yuh-Lien Chen, Department of Anatomy and Cell Biology, College of Medicine, National Taiwan University, No. 1, Sec. 1, Jen Ai Road, Taipei, 10051, Taiwan, Republic of China, Tel +886-2-23123456-288176, Fax +886-2-33931713, Email ylchenv@ntu.edu.tw; Jaw-Shiun Tsai, Department of Family Medicine, National Taiwan University Hospital, No. 1, Changde Street, Taipei, 10048, Taiwan, Republic of China, Tel +886-2-23123456-265147, Fax +886-2-23118674, Email jawshiun@ntu.edu.tw

Purpose: Particulate matter (PM) 2.5, harmful air pollutants, and diabetes are associated with high morbidity and mortality from cardiovascular disease (CVD). However, the molecular mechanisms underlying the combined effects of PM and diabetes on CVD remain unclear.

Methods: Endothelial cells (ECs) treated with high glucose (HG) and PM mimic hyperglycemia and air pollutant exposure in CVD. Endothelial inflammation was evaluated by Western blot and immunofluorescence of ICAM-1 expression and monocyte adhesion. The mechanisms underlying endothelial inflammation were elucidated through MitoSOX Red analysis, JC-1 staining, MitoTracker analysis, and Western blot analysis of mitochondrial fission-related, autophagy-related, and mitophagy-related proteins. Furthermore. nanocurcumin (NCur) pretreatment was used to test if it has a protective effect.

Results: ECs under co-exposure to HG and PM increased ICAM-1 expression and monocyte adhesion, whereas NCur pretreatment attenuated these changes and improved endothelial inflammation. PM exposure increased mitochondrial ROS levels, worsened mitochondrial membrane potential, promoted mitochondrial fission, induced mitophagy, and aggravated inflammation in HG-treated ECs, while NCur reversed these changes. Also, HG and PM-induced endothelial inflammation is through the JNK signaling pathway and miR-221/222 specifically targeting ICAM-1 and BNIP3. PM exposure also aggravated mitochondrial ROS levels, mitochondrial fission, mitophagy, and endothelial inflammation in STZ-induced hyperglycemic mice, whereas NCur attenuated these changes.

Conclusion: This study elucidated the mechanisms underlying HG and PM-induced endothelial inflammation in vitro and in vivo. HG and PM treatment increased mitochondrial ROS, mitochondrial fission, and mitophagy in ECs, whereas NCur reversed these conditions. In addition, miR-221/222 plays a role in the amelioration of endothelial inflammation through targeting Bnip3 and ICAM-1, and NCur pretreatment can modulate miR-221/222 levels. Therefore, NCur may be a promising approach to intervene in diabetes and air pollution-induced CVD.

Keywords: particulate matter, high glucose, mitochondrial fission, endothelial inflammation, miR-221/222, nanocurcumin

Received: 29 August 2023
Accepted: 27 November 2023
Published: 6 December 2023

Introduction

Air pollution is strongly associated with high morbidity and mortality from cardiovascular disease (CVD).[1] Particulate matter 2.5 (PM2.5) is the primary harmful component of air pollution, causing complications detrimental to human health worldwide.[2] An epidemiological study showed that exposure to ambient air pollutants was associated with a higher incidence of heart failure.[3] Meanwhile, hyperglycemia is a symptom of diabetes, a chronic metabolic disease, and vascular complications of diabetes lead to high cardiovascular mortality.[4] Epidemiological analyses have shown an association between diabetes and exposure to ambient air pollutants.[5,6] Furthermore, diabetes enhanced susceptibility to air pollution-related impaired vascular reactivity and endothelial function.[7] However, the mechanisms of endothelial injury caused by the combination of air pollutants and diabetes remain poorly understood.

Endothelial inflammation is critical for the development and progression of CVD.[8] Endothelial inflammation mediated by PM2.5 or high glucose has been demonstrated in previous reports.[9,10] However, the underlying mechanisms of endothelial inflammation may involve oxidative stress, mitochondrial dynamics, and autophagy in endothelial cells. PM2.5 or high glucose treatment alone is associated with oxidative stress,[11,12] mitochondrial fission,[13,14] and autophagy[15,16] and further enhances endothelial inflammation. A cohort study suggested that the intake of antioxidant-rich foods may reduce the risk of CVD mortality associated with long-term air pollution exposure,[17] suggesting that oxidative stress is a major contributor to air pollution exacerbating CVD. In addition, mitochondrial oxidative stress is associated with mitochondrial fission, further promoting CVD progression.[18] Moreover, emerging evidence suggests that autophagy, a cellular pathway responsible for the degradation of proteins and organelles, plays a key role in maintaining health and preventing diseases.[19,20] Especially, mitophagy, a macroautophagic response specifically targeting dysfunctional or cytotoxic mitochondria, represents a key bioenergetic role in the cardiovascular system and is therefore critical for cardiovascular homeostasis in health and disease.[21,22] Recent studies have shown that PM2.5 exposure induces aortic fibrosis through PINK1/Parkin-mediated mitophagy,[23] and endothelial dysfunction in diabetic patients is associated with mitophagy activation.[24] Two major mitophagy pathways are the NIX/BNIP3 pathway and the PINK1/Parkin pathway.[22] However, the precise mechanisms underlying the effects of PM on HG-treated ECs, including the roles of oxidative stress, mitochondrial dynamics, and mitophagy, as well as the complex relationships between them, remain to be elucidated. Further research is essential to fully understand these processes and their impact on cardiovascular health.

Aberrant microRNA (miR) expression is associated with CVD, and these miRNAs are transported in the blood circulation by carrier molecules, such as high-density lipoprotein (HDL), argonaute-2, and exosomes,[25] making them highly stable and suitable as disease biomarkers, such as cancer, diabetes mellitus, and CVD.[26–28] miR-221/222 is one of them.[29] miR-221/222 are clustered miRs sharing the same seed sequence, and their role in CVD is controversial. Some studies have linked miR-221/222 to cardiac hypertrophy.[30,31] In contrast, others have attributed cardioprotective effects to miR-221/222.[32,33] Furthermore, our previous reports showed that miR-221/222 is involved in TNF-α-induced ICAM-1 expression and inflammation, highlighting its role in inflammatory processes.[34,35] However, the role of miR-221/222 on endothelial function in terms of mitophagy and inflammation remains largely unknown. Further studies are critical to unravel the intricate relationship between miR-221/222, endothelial function, mitophagy, and inflammation in the context of CVD.

Curcumin, an active polyphenol compound in turmeric derived from *Curcuma longa*, has great potential for health benefits. However, its utility has been limited due to poor pharmacokinetic profile and low bioavailability, and nanocurcumin (NCur) was developed to overcome these obstacles.[36] Previous studies have shown that NCur can enhance glucose uptake and improve glucose metabolism in animal models of diabetes,[37,38] suggesting its effectiveness in improving diabetes. However, little is known about the protective mechanism of NCur against ECs simultaneously exposed to hyperglycemia and PM. This study aimed to explore the protective mechanism of NCur on ECs exposed simultaneously to HG and PM. The findings revealed that PM exacerbates the production of mitochondrial reactive oxygen species (ROS), mitochondrial fission, mitophagy, and inflammation in ECs treated with HG. Importantly, NCur attenuated HG and PM-induced mitochondrial fission, mitophagy, and inflammation by scavenging mitochondrial ROS.

Materials and Methods

PM Preparation

The PM used in this study is a standard reference material (SRM 2786) with an average particle size of <4 μm. It was collected from Prague, Czech Republic, in 2005 and bought from the National Institute of Standards and Technology (NIST, USA). The certificate and compositional analysis of SRM 2786 has been presented in a previous report.[39] To prepare SRM2786 stock solution, they were dissolved in cell culture medium and sonicated three times for 10 min in cold water to a final concentration of 10 mg/mL, then stored frozen at −20°C. To disperse PM particles, they were vigorously vortexed for 1 min before applying to subsequent experiments.

Preparation and Characterization of Curcumin Nanoparticles

Curcumin was purchased from Sigma Chemical Company (MO, USA). Nano-curcumin (NCur) was prepared by modifying a previous report.[40] To synthesize NCur, prepare a solution (0.018 M) by dissolving 198 mg curcumin in 30 mL of dichloromethane. After that, 1 mL of the stock solution was added dropwise to 50 mL of boiling water at a rate of 0.2 mL/min under sonication (Hielscher Ultrasonic Processor-UP100H, Germany). A stable droplet flow is important for nanoparticle formation and maintaining size uniformity. After sonication, stir the contents at 250 rpm for approximately 20 min at 90°C to obtain a clear orange solution. It was then concentrated and freeze-dried to get a powder. To observe NCur particles by transmission electron microscopy and measure their average particle size, 1 mg of lyophilized NCur powder was dissolved in 10 mL distilled water, and then a drop of aqueous curcumin nanoparticles was transferred onto a formvar-coated copper grid and air dried.

Culture and Application of Human Umbilical Vein Endothelial Cells (HUVECs)

HUVECs were purchased from the American Type Culture Collection (ATCC, MD, USA). They were maintained in M199 medium (Gibco, MA, USA) containing 10% fetal bovine serum (FBS, Gibco) at 37°C in 95% humidified air and 5% CO_2. Cells at passages 2–5 were used for subsequent experiments. At the beginning of the experiment, HUVECs were seeded in a 12-well plate/dish to reach 80% confluence and then cultured in low-serum medium (M199 medium containing 2% FBS) for 24 hr. The next day, HUVECs were incubated with 30 mM glucose (high glucose, HG) for 24 hr, followed by 10 μg/mL PM for 8 hr to simulate exposure to hyperglycemia and air pollution. Cells were randomly assigned to the following experimental groups: (1) control group (5.5 mM glucose), (2) PM group (10 μg/mL), (3) HG group (30mM glucose), (4) HG +PM group to assess whether PM causes severe endothelial dysfunction under hyperglycemic conditions (ie, diabetic patients). To examine the role of NCur, ROS, mitochondrial dynamics, and mitophagy in HG+PM-induced inflammation, HUVECs were pretreated with NCur (2 μM) for 12 hr or MitoQ (1 μM, Cayman, MI, USA), Mdivi-1(10 Mm, Cayman) and bafilomycin A1 (10 nM, Baf A1, Santa Cruz, TX, USA) for 1 hr.

Cell Viability Assay Using by 3-(4,5-Dimethylthiazol-2-Yl)-2,5-Diphenyltetrazolium Bromide (MTT)

To examine whether PM has the potential to enhance cytotoxicity under hyperglycemic conditions mimicking diabetes, HUVECs were incubated with HG for 24 hr and followed by treatment with 10 μg/mL PM for 8 hr to mimic hyperglycemia and air pollution. The cytotoxicity of PM and HG on HUVEC was determined by MTT assay (Sigma). 1×10^4 cells per well were seeded in 96-well plates. After different treatments, the cells were added with MTT reagent (0.5 mg/mL sterile PBS solution) and incubated at 37°C in the dark for 2 hr. Then, the medium was removed and supplemented with 50 μL of dimethyl sulfoxide (DMSO) to dissolve formazan for 30 min at 37 °C. Absorbance was measured at 570 nm by a SpctraMax ABS microplate reader (Molecular Devices, CA, USA).

$$\text{Cell viability}(\%) = \frac{\text{A570 of treated cells}}{\text{A570 of control}} \times 100\%$$

Adhesion Assay of Monocytes

HUVECs were processed in the experimental method described above. THP-1 cells, derived from human acute monocytic leukemia, were purchased from ATCC. For this experiment, THP-1 cells were labeled with 10 mM BCECF/AM (Thermo, MA, USA) for 1 hr at 37°C and then co-cultured with HUVECs for 1 hr at 37°C. Photographs of THP-1 cells adhered to HUVECs were visualized using the FLoid™ Cell Imaging Station (Thermo), and attached cells were counted using five images selected at random.

Nitric Oxide (NO) Measurement

HUVECs were subjected to the above treatments. Cells were harvested by trypsinization and incubated in RIPA buffer [50 mM Tris, pH 7.4, 150 mM NaCl, 1% NP-40, 0.5% sodium deoxycholate, and 0.1% sodium dodecyl sulfate] on ice for 20 min. Samples were centrifuged at 13,000 rpm at 4°C for 20 min, and the supernatant was subjected to a NO Assay Kit (Abcam, MA, USA). NO levels were expressed as fold changes compared to the control.

Measurement of Mitochondrial ROS Levels

Mitochondrial ROS levels were examined by MitoSOX Red (Invitrogen, MA, USA). Cells were treated for 15 min at 37°C in a medium containing 5 μM MitoSOX Red. After excitation at 510 nm, red fluorescence at 580 nm was observed by a fluorescence microscope (Leica, Wetzlar, Germany). It was also quantified by LSRFortessa flow cytometry (BD, NJ, USA).

Analysis of Mitochondrial Membrane Potential (Δψm)

JC-1 (Cayman) staining and MitoStatus TMRE (BD) staining were used to examine fluctuations in ΔΨm. Cells were treated in media containing 2 μg/mL of JC-1 in the dark for 30 min at 37°C. Green fluorescence represents the JC-1 monomer with low ΔΨm, whereas red fluorescence reflects the aggregated form with intact ΔΨm. Images were captured with a fluorescence microscope and analyzed with an LSRFortessa flow cytometer. Additionally, cells were incubated at 37°C for 15 min in media containing 100 nM MitoStatus TMRE. ΔΨm was then analyzed by LSRFortessa flow cytometry.

ATP Determination

HUVECs were processed as described above. Cells were trypsinized and lysed in RIPA buffer on ice for 20 min. Samples were centrifuged at 13,000 rpm for 20 min at 4°C, and ATP levels in the supernatant were examined by an ATP assay kit (Thermo, MA, USA). ATP levels are expressed as the fold change compared with the control.

Western Blot Analysis

The procedure for Western blot was conducted and modified as described in the previous report.[41] Cells and aortic tissues were lysed in RIPA buffer. After electrophoresis of equal amounts of protein samples (30 μg) on SDS- polyacrylamide gel, the proteins separated in the gels were transferred onto polyvinylidene fluoride (PVDF) membranes (Millipore). These membranes were immersed in 1 × TBST (10 mM Tris/150 mM NaCl/0.05% Tween-20, pH 7.5) containing 5% milk at room temperature for 1 hr to block non-specific proteins. These membranes were incubated overnight at 4°C with the following primary antibodies: ICAM-1 (1:1000, sc-8439, Santa Cruz), p-DRP1 (1:1000, 3455S, Cell Signaling, MA, USA), FIS1 (1:1000, Proteintech, IL, USA), LC3B (1:2000, 2775S, Cell Signaling), SQSTM1/p62 (1:2000, 5114S, Cell Signaling), BNIP3 (1:1000, 44060S, Cell Signaling), phospho-ERK (1:2000, sc-7383, Santa Cruz), phospho-SAPK/JNK (1:2000, 9251S, Cell Signaling), phospho-p38 MAP kinase (1:2000, 9211S, Cell Signaling), Bnip3 (rodent specific, 1:1000, 3769S, Cell Signaling), and GAPDH (1:5000, 60004-1-Ig, Proteintech). These membranes were then soaked in horseradish peroxidase-conjugated goat anti-rabbit or mouse IgG (1:5000, 111-035-144 or 115-035-003, Jackson ImmunoResearch, MA, USA) for 1 hr at RT. Immunoreactive bands were developed using LuminataTM crescendo ECL (Millipore). A Biospectrum Imaging System (UVP, CA, USA) was used to obtain images. ImageJ software (NIH, USA) was used for the densitometric analysis of Western blots. Relative levels of proteins were determined and normalized to the housekeeping protein GAPDH.

MitoTracker Staining

HUVECs were seeded at 80% confluence in 35 mm μ-Dish with 4-well culture inserts (ibidi GmbH, Gräfelfing, Germany). To measure mitochondrial length, HUVECs were treated as indicated and stained with a medium containing 400 nM MitoTracker (Thermo) for 30 min in a 37°C incubator with 5% CO_2. Images were captured by a spinning disc confocal microscope (Zeiss, Oberkochen, Germany). The mitochondrial length was calculated by measuring the average of 15 mitochondrial measurements in 10 cells per group using ImageJ software.

DRP siRNA Knockdown

HUVECs were seeded at 70% confluency in 12-well plates. Cells were then transfected with 25 nM SMARTPool siRNA targeting DRP1 (siDRP1) or scrambled siRNA (siScr) (Horizon Discovery, CO, USA) using Lipofectamine 3000 (Thermo) according to the manufacturer's instructions. The next day, cells were transferred to M199 medium containing low serum. After 24 hr, cells were transferred to M199 medium containing HG and incubated for another 24 hr. Then, cells were treated with PM (10 μg/mL) for 8 hr. After the above treatments, HUVECs were used for subsequent analysis.

Acridine Orange Staining

Acridine orange (AO, Invitrogen) solution can identify lysosomes, autolysosomes, and acidic organelles. The presence of orange-fluorescent AO in acidic vesicles can be used to observe autophagy. Cells with different treatments were incubated with media containing AO (1 μg/mL) for 30 min at 37°C. The fluorescence was assessed under a fluorescence microscope (Leica).

RNA Extraction and Quantitative Reverse Transcription PCR (RT-qPCR)

Total RNA was extracted from HUVECs or mouse aortas using TRIzol reagent (Thermo) per the manufacturer's instructions. The cDNA templates were synthesized using TaqMan MicroRNA Reverse Transcription Kit (Invitrogen). To examine the expression levels of miR-221/222, RT-qPCR was performed by using the TaqMan Universal PCR Master Mix (Applied Biosystems, CA, USA) in a QuantStudio 3 Real-Time PCR System (Thermo). TaqMan microRNA detection kits for miR-221 (000524), miR-222 (002276), and RNU6B (001973) were bought from Thermo. All reactions were performed in at least triplicate. Quantification of miR-221/222 expression levels was normalized by RNU6B expression.

Animal Model

C57BL/6 male mice, 6 weeks old, weighing 20 g, were purchased from the Experimental Animal Center of National Taiwan University and this mouse strain was obtained from The Jackson Laboratory (Stock No: 000664, Bar Harbor, ME, USA). MiR-221/222 knockout (KO) mice were generated by deleting the X-linked miR-221/222 gene and were backcrossed on a C57BL/6J background for 10 generations.[35] Mice were housed on a 12-hr light/dark cycle and provided water and food ad libitum. All animal experiments were conducted in accordance with the guidelines for the National Taiwan University College of Medicine Institutional Animal Care and Use Committee (IACUC approval no: 20180426) and followed the 3R concept. Mice were randomly divided into control, PM exposure (PM), diabetes (STZ), STZ+PM, and STZ+PM+NCur groups (7 mice in each). After mice were fasted overnight, an intraperitoneal injection of 55 mg/kg streptozotocin (STZ in 0.1 M sodium citrate buffer, pH 4.5, Sigma) induced a hyperglycemia animal model for 5 consecutive days. Mice were anesthetized with 2% isoflurane and blood samples were collected from the submandibular region, fasting blood glucose levels above 280 mg/dL were considered diabetic, and the mice were subjected to subsequent experiments. However, mice with fasting blood glucose values below 280 mg/dL required euthanasia to achieve humane endpoints. At the same time, mice of the control group and the PM group were intraperitoneally injected with sodium citrate buffer as vehicle treatment.

NCur is administered orally at a dose of 15 mg/kg every two days for two weeks. To simulate air pollution, mice were injected intratracheally with PM dissolved in PBS at 10 mg/kg under anesthesia on the first and eighth days of two weeks. First, mice were anesthetized with 2% isoflurane inhalation. The trachea was exposed, and PM was injected into the anterior wall of the trachea with an insulin syringe at a 45° angle to avoid puncturing the posterior wall. After the PM

injection, the trachea and neck were sutured, and the mice were put back into the cage after waking up. Control and STZ groups received the intratracheal injection of PBS as vehicle treatment. Mice injected intratracheally with PM did not die, and all mice survived until the end of the experiment. Serum was collected at the end of the experimental period to measure blood glucose, serum alanine aminotransferase (ALT), and creatinine levels. In addition, a portion of thoracic aortic tissue was fixed with 4% paraformaldehyde in PBS, embedded in paraffin, and subjected to immunofluorescent staining. Another part of the tissue was flash-frozen in liquid nitrogen to isolate proteins to measure expression levels of ICAM-1, p-DRP1, FIS1, LC3B, and BNIP3 or for RNA extraction to quantify miR-221/222 levels using RT-qPCR.

Immunofluorescence Staining

5 μm-thick sections from paraffin blocks of thoracic aortas were deparaffinized in an oven at 60°C for 1 hr and then rehydrated with graded alcohols. Antigen retrieval was used with 10 mM sodium citrate. Sections were first stained with ICAM-1 (diluted 1:100, sc-8439, Santa Cruz) antibody at 4°C overnight and then stained with CD31 (endothelial cell marker, 1:200, ab28364, Abcam) antibody at 4°C overnight to determine if ICAM-1 is expressed by ECs. Subsequently, sections were immersed in Alexa Fluor 488-conjugated secondary antibody (1:200 dilution, A-11001, Thermo) and Alexa Fluor 594-conjugated secondary antibody (1:200 dilution, A-11012, Thermo) at room temperature for 1 hr, the expression of ICAM-1 and CD31 were detected respectively. Slides were then counterstained with DAPI, and images were captured by an ApoTome fluorescence microscope (Zeiss).

Detection of Mitochondrial ROS Production in the Aorta

Mouse aortas were immersed with OCT (Fisher Scientific, MA, USA), and 10 μm cryosections were cut using a cryostat (Leica). The sections were incubated with 5 μM MitoSOX Red for 15 min at 37°C. Nuclei were counterstained with DAPI. The images were visualized and captured using a fluorescence microscope.

Transmission Electron Microscopy

Mouse thoracic aorta tissue was fixed overnight at 4°C with 2% glutaraldehyde and 2% paraformaldehyde fixative. After washing with PBS, samples were postfixed with 1% osmium tetroxide (OsO_4), dehydrated in graded alcohols, and embedded in Epon. Uranyl acetate and lead citrate were used to stain ultrathin sections. The ultrastructure was observed by an H-7500 transmission electron microscope (Hitachi, Japan), and photographs were acquired by AMT Image Capture Engine V5.4.2 (Advanced Microscopy Techniques, MA, USA).

Statistical Analysis

Each in vitro experimental group contained five independent biological replicates. In vivo studies used seven animals per group. Data are expressed as mean ± S.E.M. Statistical analysis was performed using SPSS software (version 17.0; IBM, New York, USA). Data were checked for homogeneity and normality using Bartlett's test and Shapiro–Wilk test, respectively, before performing one-way analysis of variation (ANOVA). ANOVA with Dunnett's post hoc test was used for multiple comparisons. Differences between the two groups were determined using Student's *t*-test. $P<0.05$ represents statistical significance.

Results

PM Impaired Cell Viability and Induced Inflammation on HG-Treated ECs and NCur Reversed These Effects

ECs treated with 10, 20, or 30 mM glucose alone for 32 hr did not induce marked cytotoxicity (Figure 1A). ECs treated with 10 μg/mL of PM alone for 8 hr decreased cell viability compared to control cells. Furthermore, ECs were pretreated with 30 mM glucose (high glucose, HG) for 24 hr and then treated with 10 μg/mL PM for 8 hr (HG+PM); a marked reduction in cell viability was detected compared to the cells treated with HG or PM alone (Figure 1A and B). After that, cells were incubated with HG for 24 hr, followed by 10 μg/mL PM treatment for 8 hr, and then applied to Western blot to examine the inflammation of HUVECs under different treatments. ECs incubated with HG and PM alone significantly

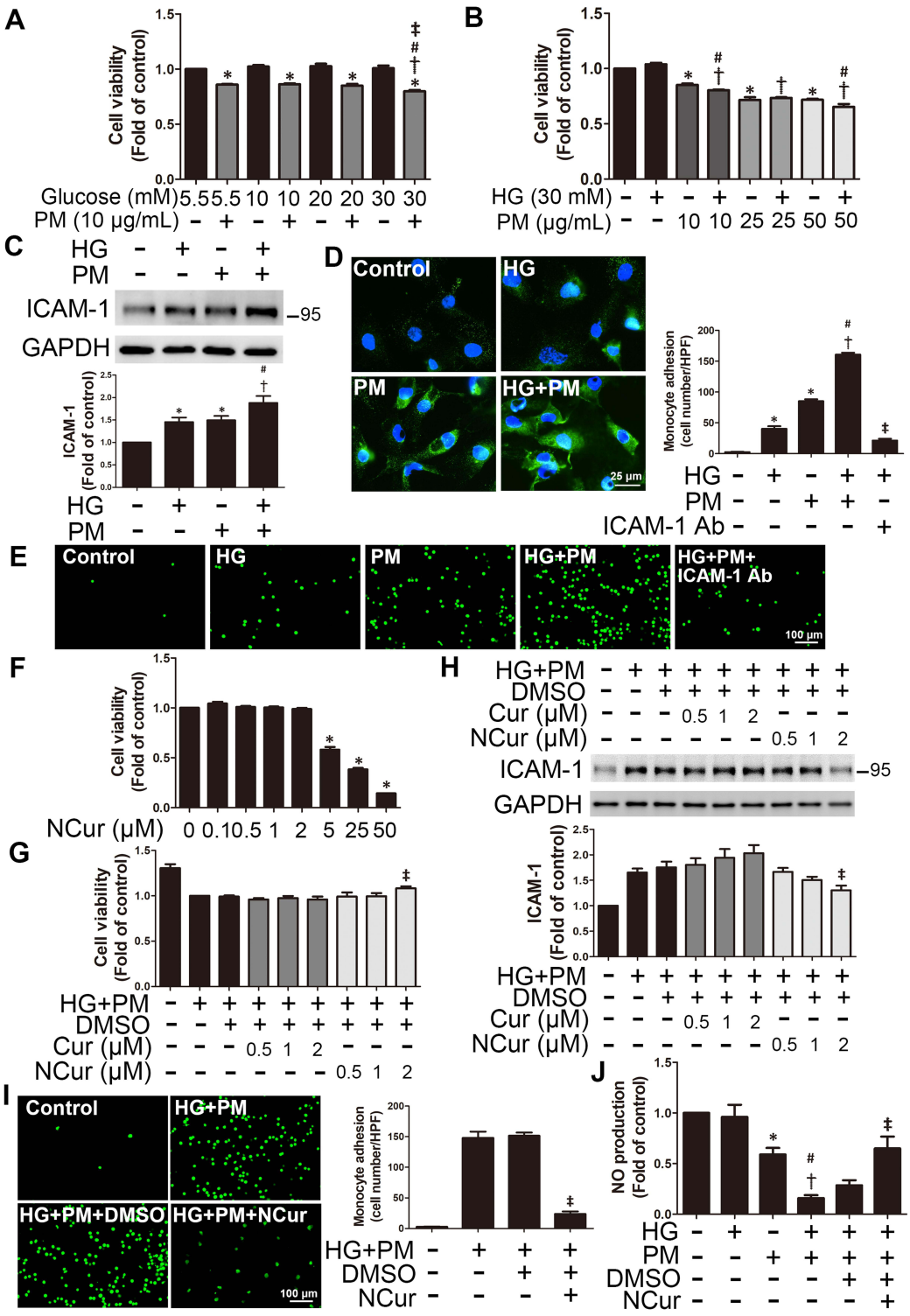

Figure 1 PM impaired cell viability and induced ICAM-1 expression in HG-treated ECs, whereas NCur reversed these effects.

Notes: (**A**) HUVECs were pretreated with different concentrations of glucose for 24 hr, and then treated with or without 10 μg/mL PM for 8 hr. The cell viability was assessed by MTT assay. (**B**) HUVECs were pretreated with or without HG (30 mM) for 24 hr, and then treated with or without different concentrations of PM for 8 hr. MTT assay was used to assess the cell viability. (**C** and **D**) HUVECs were pretreated with HG for 24 hr, and then treated with or without PM for 8 hr. The level of ICAM-1 expression was detected by Western blot and by immunofluorescent staining (nuclei: blue; bar=25 μm). (**E**) Representative fluorescent images showing the attachment of fluorescein-labeled THP-1 cells to HUVECs. ICAM-1 antibody was pretreated 12 hr before PM exposure. (**F**) HUVECs were treated with different concentrations of nanocurcumin (NCur) for 24 hr, and then the cell viability was assessed by MTT assay. (**G**) HUVECs were pretreated without or with different concentrations of curcumin (Cur) or with NCur for 24 hr, pretreated with HG for 24 hr, and then treated with PM for 8 hr. The cell viability was assessed by MTT assay. (**H**) The effects of Cur and NCur on the level of ICAM-1 expression were detected by Western blot. (**I**) Effect of NCur on the fluorescein-labeled THP-1 cells adhering to HG+PM-treated HUVECs. (**J**) Effect of NCur on NO production in HG+PM-treated HUVECs. N=5. $^{*}P$ <0.05 compared with the glucose 5.5, 10, 20, and 30 mM group, control group or NCur 0 μM group; $^{\dagger}P$ <0.05 compared with the HG group or HG 5.5 mM+PM group; $^{\#}P$ <0.05 compared with the PM group or HG 10 mM+PM group; $^{\ddagger}P$ <0.05 compared with the HG 20 mM+PM group, HG+PM group or HG+PM+DMSO group.

increased the ICAM-1 expression. The level of ICAM-1 was also significantly elevated in the HG+PM group when compared with HG or with PM alone (Figure 1C). Consistent with the Western blot results, the ICAM-1 expression was more robust in the HG+PM group when compared with HG or with PM alone by immunofluorescent staining (Figure 1D). Since cell adhesion molecules are critical for monocyte adhesion, the effects of HG and PM on this adhesion were studied. Treatment with HG or PM alone increased the number of monocytes adhered to HUVECs, and HG+PM treatment together resulted in a significant increase in monocyte binding compared to a single treatment (Figure 1E). Furthermore, ICAM-1 neutralizing antibody pretreatment significantly decreased the number of monocytes attaching to HG+PM-treated ECs (Figure 1E). We also evaluated the effects of curcumin (Cur) and nanocurcumin (NCur) on cell viability and inflammation of HG and PM-treated ECs. We found that NCur at 2 μM increased cell viability and decreased ICAM-1 expression by HG and PM treatment, while Cur had no effect (Figures 1F–H). We also found that NCur decreased the monocytes adhered to ECs by HG and PM treatment (Figure 1I). NCur increased nitric oxide (NO) production, a hallmark of endothelial function, in HG+PM-treated ECs (Figure 1J). These results suggested that PM aggravated the effects of HG on the endothelial viability and inflammation.

PM Exacerbated Mitochondrial ROS Production in HG-Treated ECs, and NCur Reversed the Effect

ROS production, mainly generated from mitochondria, is a crucial step in developing numerous inflammatory disorders.[42] The levels of mitochondrial ROS were assessed by the MitoSOX Red assay. As shown in Figure 2A, HG or 10 μg/mL PM alone caused a slight fluorescence. Cells were incubated with HG for 24 hr, followed by 10 μg/mL PM exposure for 8 hr, and MitoSOX Red staining showed a significant increase in mitochondrial ROS fluorescence. Consistent with the results, the HG+PM group showed a considerable fluorescence value compared with the groups that received HG or PM alone by flow cytometry (Figure 2B). HG+PM-induced mitochondrial ROS expression was inhibited by the mitochondrial-targeted antioxidant mitoquinol (MitoQ) (Figure 2A and B). Next, we assessed whether the level of ICAM-1 expression in HG+PM-treated ECs was triggered by the upregulation of mitochondrial ROS. The data exhibited that MitoQ pretreatment decreased the ICAM-1 expression level and the number of monocyte adhesion in HG+PM-treated ECs (Figure 2C and D). As shown in Figure 2E, pretreatment with NCur significantly reduced HG+PM-induced mitochondrial ROS production via fluorescence microscopy. Moreover, flow cytometry analysis was consistent with them (Figure 2F). Thus, these data show that mitochondrial ROS production is indispensable for HG+PM-induced ICAM-1 expression in ECs and that NCur reduced this effect.

HG and PM Significantly Reduced Δψm and Increased Mitochondrial Fission, Whereas NCur Reversed These Effects

Mitochondria utilize cycles of fusion and fission for dynamic membrane remodeling under normal physiological conditions. Dysregulation of mitochondrial fission and fusion plays a key role in the pathogenesis of many diseases.[43] As a result of mitochondrial ROS production in HG+PM-treated cells, we assessed several mitochondrial functions, including changes in mitochondrial membrane potential (ΔΨm), ATP production, and levels of mitochondrial fission-related proteins. ΔΨm and ATP levels are important factors of mitochondrial and cellular function. The JC-1 assay showed a significant shift in fluorescence emission from red to green in ECs treated with HG+PM, a shift indicative of a decrease in ΔΨm (Figure 3A). In addition, analysis of JC-1 result using flow cytometry showed that HG+PM treatment decreased the ratio of red to green MFI (mean fluorescence intensity) (Figure 3B). MitoStatus TMRE is a positively charged dye that binds to negatively charged mitochondria and fluoresces red. From the MitoStatus TMRE flow cytometry results, we found that the ΔΨm was significantly decreased in the HG or PM alone treatment group compared with the control group. ΔΨm was also significantly lower in the HG+PM group than in the PM alone or the HG alone groups (Figure 3C). Furthermore, ATP content remarkably decreased after HG+PM treatment (Figure 3D).

MitoTracker was used to specifically stain and examine changes in mitochondrial morphology. We observed that mitochondrial length was significantly decreased in HG+PM-treated cells compared to cells treated with HG or PM alone (Figure 3E). The expression of p-DRP1 and FIS1, mitochondria fission-related proteins, was remarkably increased after

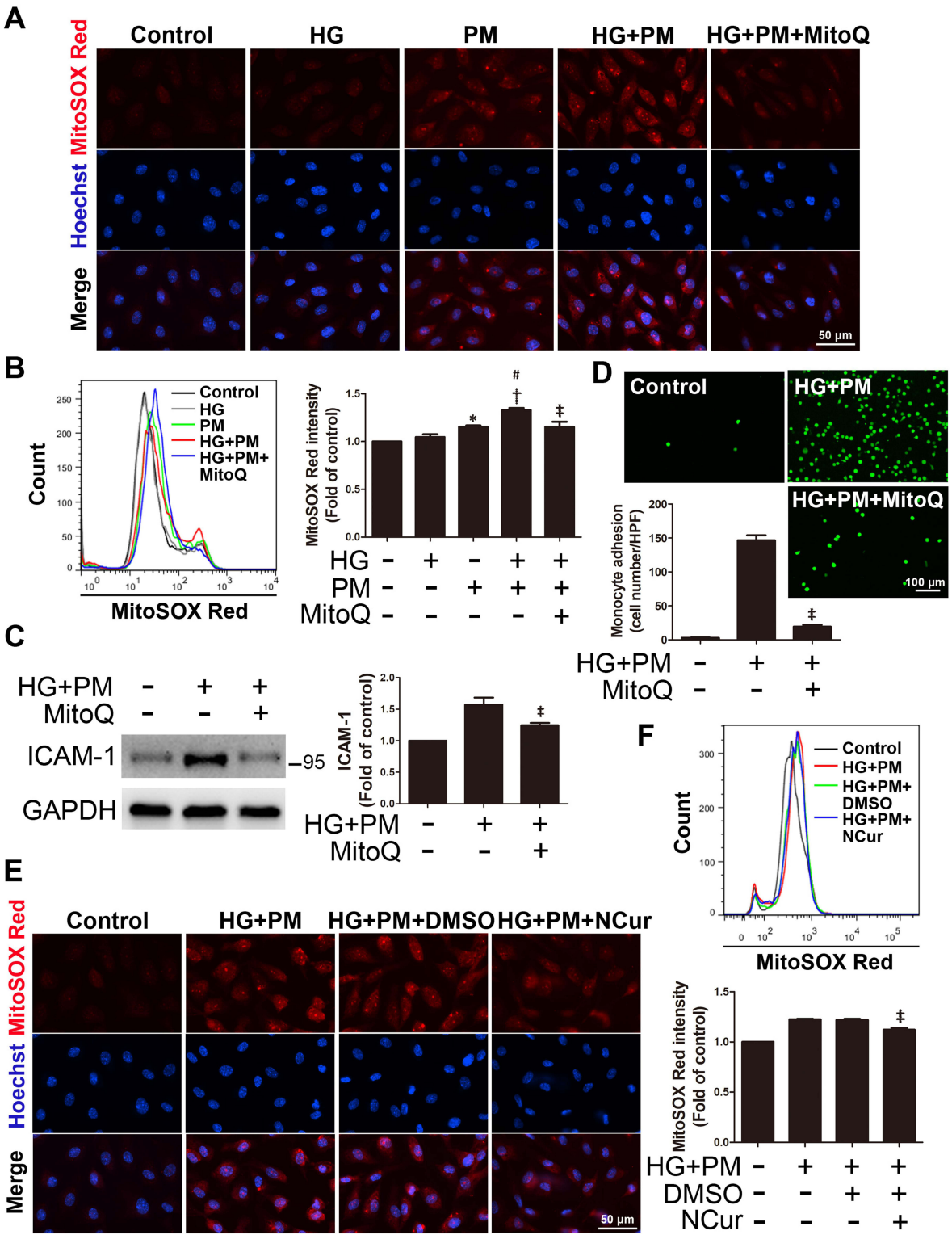

Figure 2 PM exacerbates ROS production in ECs treated with HG, and NCur pretreatment reduces the effect.

Notes: HUVECs were pretreated with HG (30 mM) for 24 hr, and then treated with PM (10 μg/mL) for 8 hr. Before exposure to PM, HUVECs were pretreated with 1 μM MitoQ or with 2 μM NCur for 1 hr or 12 hr, respectively. (**A** and **B**) Mitochondrial ROS was detected by MitoSOX Red staining under a fluorescence microscope and analyzed using flow cytometry. (**C**) The effect of MitoQ pretreatment on the level of ICAM-1 expression was determined using Western blot. (**D**) The effect of MitoQ pretreatment on the adhesion of fluorescein dye-labeled THP-1 monocytes to HG+PM-treated HUVECs. (**E** and **F**) HUVECs were pre-treated with HG for 24 hr, and then incubated with 2 μM NCur for 12 hr before exposure to PM. The effect of NCur on mitochondrial ROS was detected by MitoSOX Red under fluorescence microscopy and flow cytometry. Bar=50 μm. N=5. $^{*}P$ <0.05 compared with the control group; $^{\dagger}P$ <0.05 compared with the HG group; $^{\#}P$ <0.05 compared with the PM group; $^{\ddagger}P$ <0.05 compared with the HG+PM group.

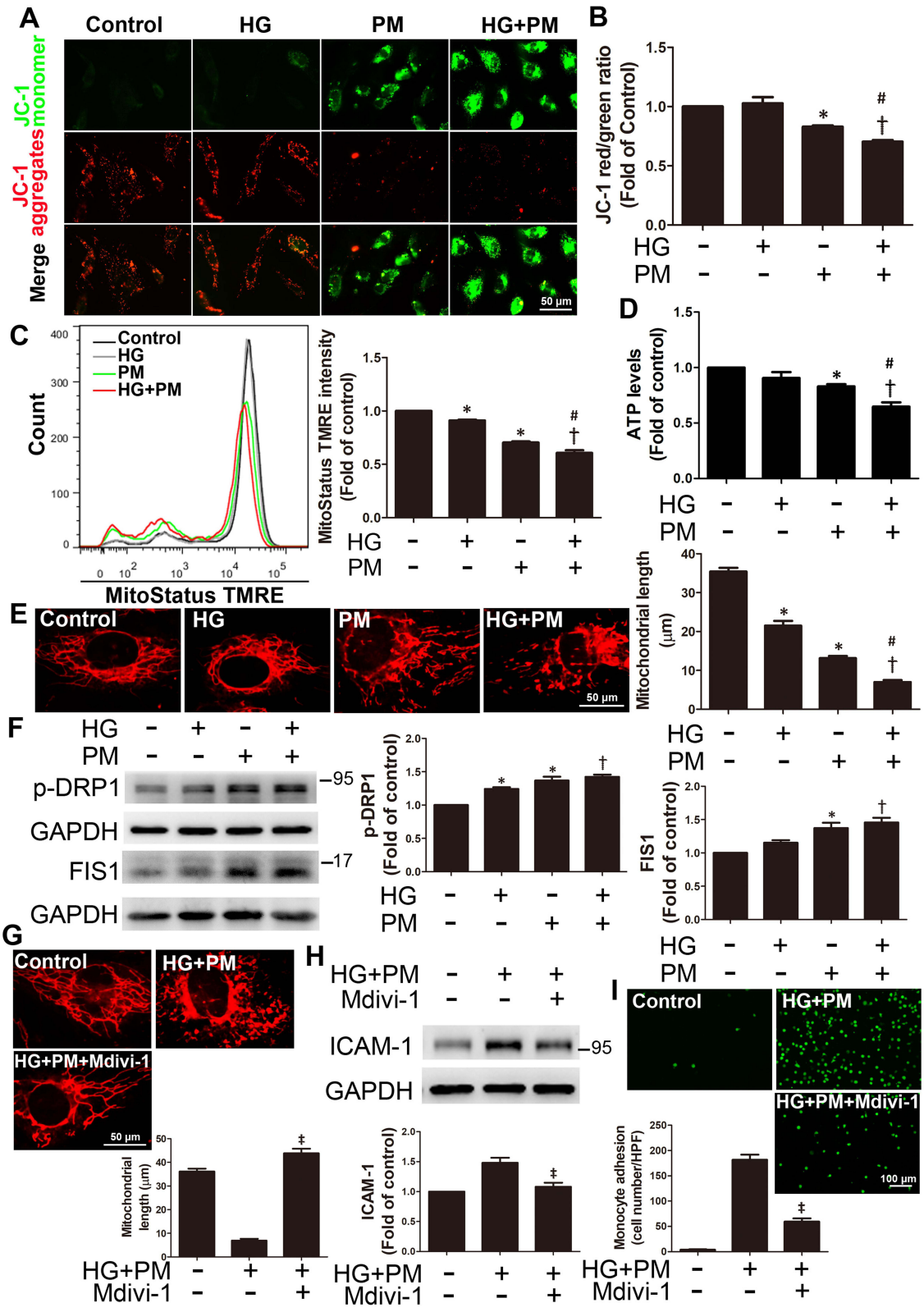

Figure 3 Continued.

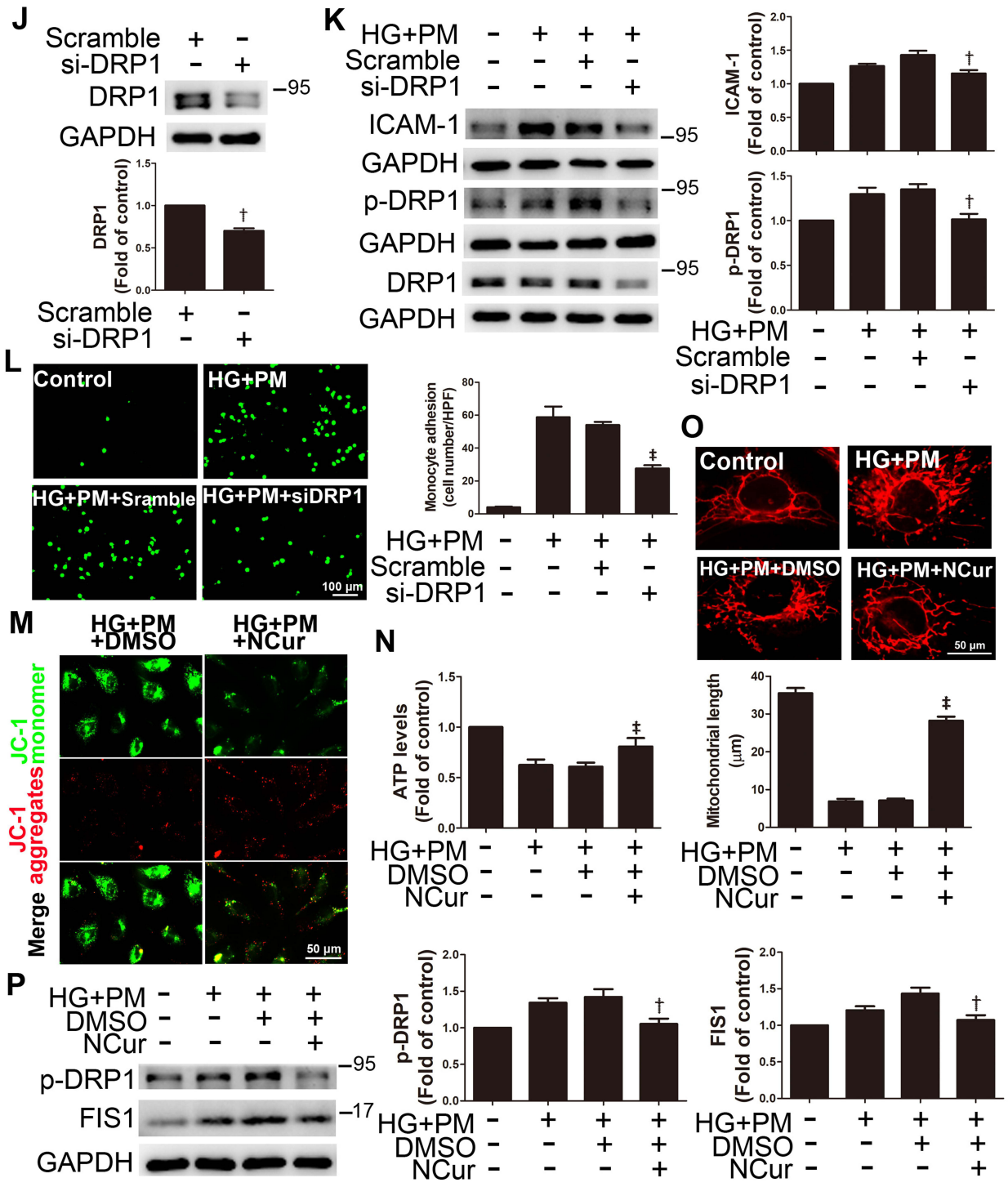

Figure 3 PM aggravated mitochondrial injury and mitochondrial fission in ECs treated with HG, and NCur pretreatment reduced this change.

Notes: HUVECs were pretreated with HG for 24 hr and then treated with PM for 8 hr. Some HUVECs were pretreated with 10 μM Mdivi-1 or 2 μM NCur for 1 hr or 12 hr, respectively before PM exposure. (**A** and **B**) JC-1 assay was used to examine mitochondrial membrane potential (ΔΨm) by fluorescence microscopy and by flow cytometry. The JC-1 ratio (aggregate/monomer ratio) was used for quantitative analysis of ΔΨm. Bar= 50 μm. (**C**) MitoStatus TMRE dye was used for the quantitative analysis of ΔΨm with flow cytometry. (**D**) ATP level was determined by the ATP assay. (**E**) Mitochondrial length was determined using MitoTracker staining. Bar= 50 μm. (**F**) The expression of mitochondrial fission-related proteins, phosphorylated DRP1 (Ser 616) and FIS1, was assessed by Western blot. (**G**) The effect of Mdivi-1 pretreatment on mitochondrial length in HG+PM-treated cells was analyzed by MitoTracker staining. (**H**) The effect of Mdivi-1 on ICAM-1 expression was evaluated using Western blot. (**I**) The effect of Mdivi-1 pretreatment on adhesion of fluorescein-labeled THP-1 monocytes to HUVECs. (**J**) The efficiency of DRP1 knockdown was determined using Western blot. (**K**) Western blot was used to examine the effect of DRP1 knockdown on the expression of ICAM-1, p-DRP1 and DRP1. (**L**) The effect of DRP1 knockdown on the adhesion of fluorescein-labeled THP-1 monocytes to HUVECs. (**M**) The effect of NCur on ΔΨm in HG+PM-treated HUVECs. (**N**) The effect of NCur on ATP production in HG+PM-treated HUVECs. (**O**) The effect of NCur on mitochondrial length in HG+PM-treated HUVECs. (**P**) The effect of NCur on the expression of mitochondrial fission-related proteins p-DRP1 and FIS1 was determined using Western blot. N=5. **P* <0.05 compared with the control group; †*P* <0.05 compared with the HG group; #*P* <0.05 compared with the PM group; ‡*P* <0.05 compared with the HG+PM group.

HG+PM stimulation (Figure 3F). Mdivi-1, a mitochondrial fission inhibitor, was applied to explore whether the inflammatory responses are triggered by HG+PM-induced mitochondrial fission. Pretreatment with Mdivi-1 significantly increased mitochondrial length (Figure 3G). Mdivi-1 pretreatment also reduced ICAM-1 expression and the number of adherent monocytes increased by HG+PM treatment (Figures 3H and I). Western blot showed that DRP1 siRNA efficiently reduced endogenous levels of DRP1 (Figure 3J). DRP1 knockdown significantly decreased HG+PM-induced ICAM-1 expression (Figure 3K) and monocyte adhesion (Figure 3L).

NCur treatment augmented ΔΨm when compared with the HG+PM group by JC-1 staining (Figure 3M). Moreover, NCur treatment significantly increased the ATP level compared to the HG+PM group (Figure 3N). NCur treatment significantly increased the length of HG+PM-reduced mitochondrial length by MitoTracker staining (Figure 3O). HG +PM-induced expression of p-DRP1 and FIS1 was significantly decreased by NCur treatment (Figure 3P). These results suggested that HG+PM induced ICAM-1 expression by increasing mitochondrial fission in ECs. Conversely, NCur attenuated this effect.

PM Aggravated Mitophagy in HG-Treated ECs, Whereas NCur Reversed the Effect

Mitochondrial ROS production leads to mitochondrial damage. Damaged mitochondria are selectively encapsulated in autophagosomes, which subsequently fuse with nearby lysosomes to form autolysosomes. These processes are called mitophagy.[44] Autolysosomes exhibit red fluorescence via the AO staining. We found that the combined exposure of HG and PM treatments increased red fluorescence (Figure 4A). PM treatment increased the expression of autophagy-related proteins p62 and LC3B, and mitophagy-related protein BNIP3, and the co-exposure to PM and HG has an additive effect on the levels of p62, LC3B, and BNIP3 expression (Figure 4B). MitoQ or Mdivi-1 treatment suppressed red fluorescence by AO staining (Figure 4C). Here, MitoQ or Mdivi-1 attenuated the increase of these autophagy-related and mitophagy-related proteins upregulated by HG and PM treatment (Figure 4D). NCur treatment significantly decreased autolysosomes when compared with the HG+PM group by AO staining (Figure 4C). Moreover, HG+PM-induced expression of p62, LC3B, and BNIP3 was significantly decreased by NCur treatment (Figure 4D). Next, we used bafilomycin A1 (Baf. A1) to study whether NCur reduces inflammation via repression of HG+PM-induced mitophagy. Baf. A1 inhibits fusion between autophagosomes and lysosomes and blocks vacuolar H^+-ATPase, thereby inhibiting autolysosome formation.[45] Baf. A1 pretreatment significantly increased HG+PM-induced ICAM-1 expression and monocyte adhesion (Figure 4E and F). These results suggested that HG+PM induced ICAM-1 expression by increasing mitophagy in ECs. In contrast, NCur attenuated ICAM-1 expression by reducing HG+PM-induced mitophagy.

Co-Exposure of PM and HG Induced Inflammation and Mitophagy via JNK Signaling Pathways, and NCur Reversed These Effects

We investigated whether cells treated with HG and PM lead to inflammation and mitophagy induced by the MAPK signaling pathway. HUVECs were incubated with PM under HG conditions for the indicated duration (0, 0.5, 1, 2 hr). We found that under HG conditions, the levels of p-JNK, p-ERK, and p-p38 expression were significantly upregulated after 0.5, 1, and 2 hr of PM exposure, respectively (Figure 5A). NCur decreased HG+PM-induced p-JNK expression. Then, HUVECs were pretreated with specific inhibitors of ERK (PD98059), JNK (SP600125), and p38 (SB203580) for 1 hr before exposure to PM. SP600125 reduced mitochondrial ROS by MitoSOX staining (Figure 5B), attenuated ΔΨm collapse by JC-1 staining (Figure 5C), and significantly increased the mitochondrial length in HG+PM-treated ECs by MitoTracker staining (Figure 5D). However, pretreatment with PD98059 and SB203580 did not affect these changes induced by HG+PM. Furthermore, SP600125 suppressed red fluorescence by AO staining (Figure 5E). Next, ICAM-1 expression levels were reduced under the pretreatment of SP600125 but not changed under the pretreatment of PD98059 and SB203580 (Figure 5F). The levels of p-DRP-1, p62, LC3B, and BNIP3 were decreased under SP600125 pretreatment. In contrast, the levels of these proteins were unchanged under PD98059 and SB203580 pretreatment (Figure 5F). SP600125 significantly reduced the number of monocytes adhered to ECs with HG and PM treatment (Figure 5G). These

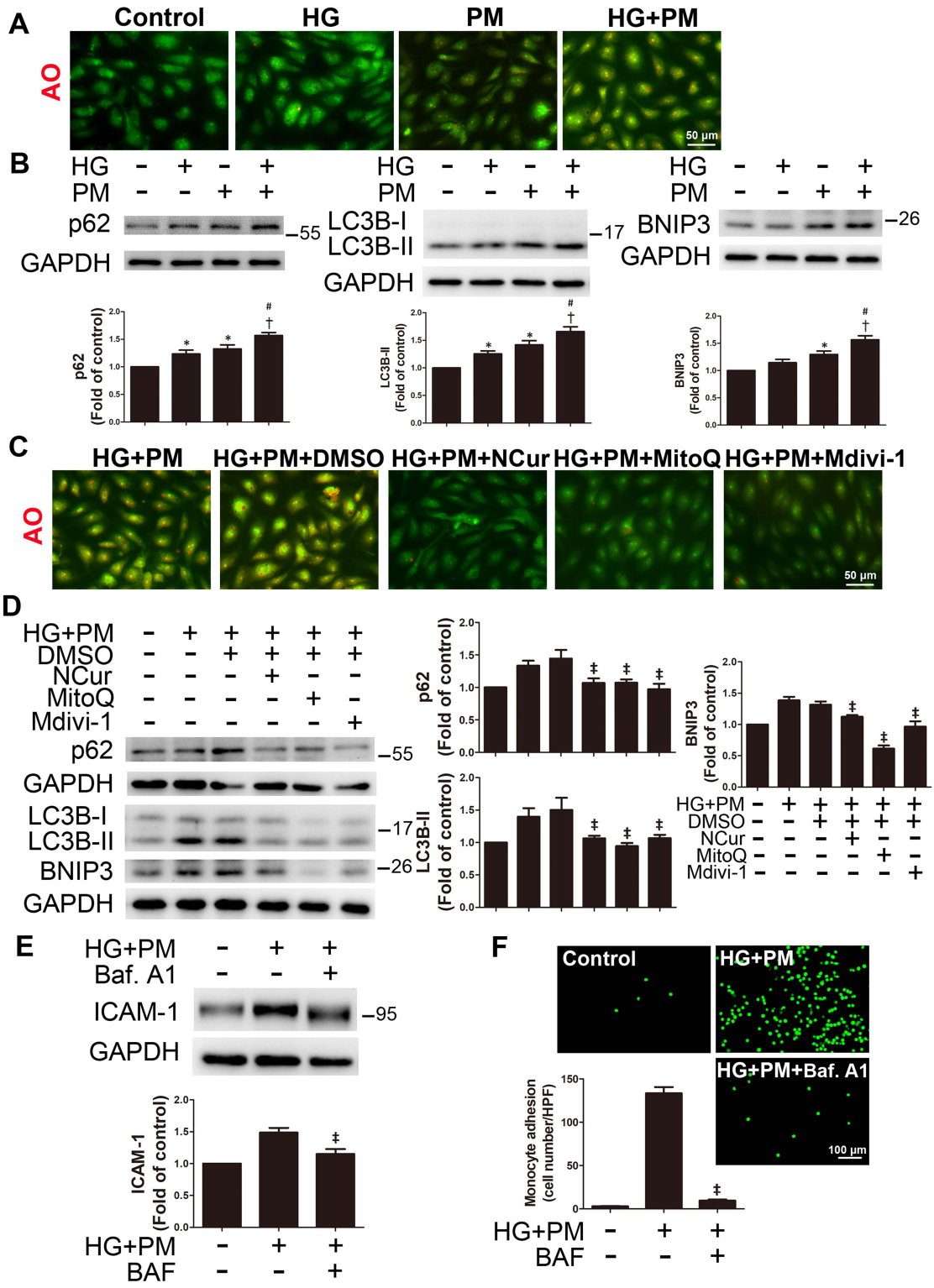

Figure 4 PM aggravated mitophagy in ECs treated with HG, and NCur reversed the effect.

Notes: HUVECs were pretreated with HG (30 mM) for 24 hr and then treated with PM (10 μg/mL) for 8 hr. Before exposure to PM, HUVECs were pretreated with 1 μM MitoQ, 10 μM Mdivi-1, 100 nM Bafilomycin A1 (Baf. A1) for 1 hr or 2 μM NCur for 12 hr, respectively, before PM exposure. (**A**) AO staining detects the formation of autolysosomes, which appear red fluorescence under a fluorescence microscope. Bar=50 μm. (**B**) Western blot was used to detect the expression levels of p62, LC3B and BNIP3. (**C**) The effects of NCur, MitoQ and Mdivi-1 on the formation of autolysosome were determined by AO staining. Bar=50 μm. (**D**) The effects of NCur, MitoQ and Mdivi-1 on the expression of autophagy-related and mitophagy-related proteins were determined by using Western blot. (**E**) The effect of Baf. A1 on ICAM-1 expression in HG+PM-treated HUVECs was determined by Western blot. (**F**) The effect of Baf. A1 pretreatment on adhesion of fluorescein-labeled THP-1 monocytes to HG+PM-treated HUVECs. N=5. $^{*}P$ <0.05 compared with the control group; $^{\dagger}P$ <0.05 compared with the HG group; $^{\#}P$ <0.05 compared with the PM group; $^{\ddagger}P$ <0.05 compared with the HG +PM group.

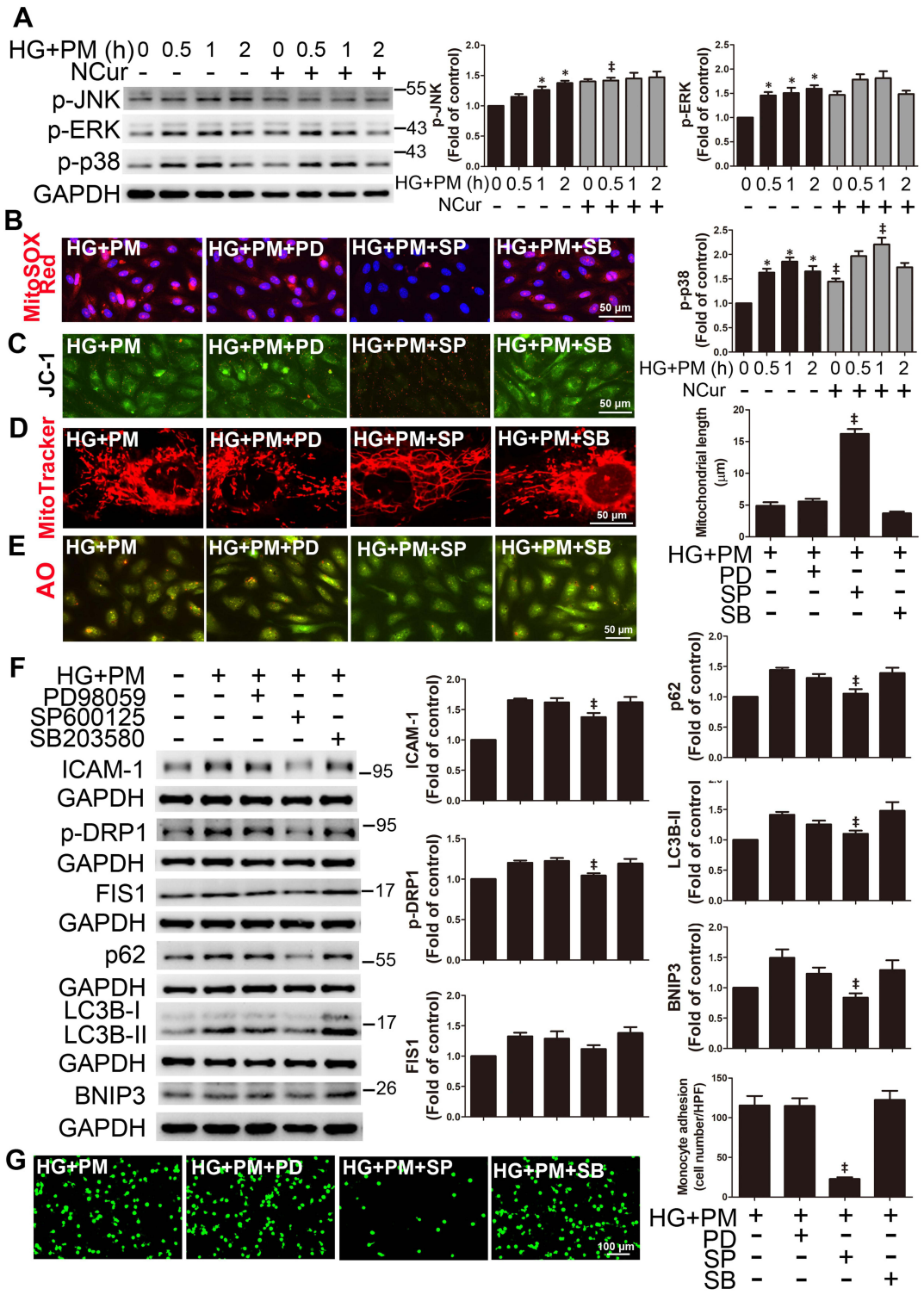

Figure 5 Co-exposure to PM and HG induced inflammation and mitophagy via JNK signaling pathway, and NCur reversed these effects.

Notes: HUVECs were pretreated with HG (30 mM) for 24 hr and then treated with PM (10 μg/mL) for 8 hr. HUVECs were pretreated with 10 μM PD98059, 10 μM SP600125, and 10 μM SB203580 for 1 hr or with 2 μM NCur for 12 hr before PM exposure. (**A**) Expression levels of p-ERK, p-p38, and p-JNK were examined at different time points (0, 0.5, 1, and 2 hr) by Western blot. (**B**) The effect of MAPK inhibitors on mitochondrial ROS in HG+PM-treated HUVECs were detected by MitoSOX Red staining under a fluorescence microscope. Bar=50 μm. (**C**) The effect of MAPK inhibitors on ΔΨm in HG+PM-treated HUVECs were detected by JC-1 staining under a fluorescence microscope. Bar=50 μm. (**D**) The effect of MAPK inhibitors on mitochondrial length in HG+PM-treated HUVECs were determined by MitoTracker staining under a spinning disc confocal microscope. Bar=50 μm. (**E**) The effect of MAPK inhibitors on the autolysosome formation in HG+PM-treated HUVECs. Bar=50 μm. (**F**) The effects of MAPK inhibitors on the levels of mitochondrial fission-related proteins, p-DRP and FIS1, autophagy-related proteins p62 and LC3B-II and mitophagy-related protein BNIP3, and inflammation-related protein, ICAM-1 expression were examined using Western blot. (**G**) The effect of MAPK inhibitors on fluorescein dye-labeled THP-1 monocytes adhered to HG+PM-treated HUVECs. N=5. **P* <0.05 compared with the control group; ‡*P* <0.05 compared with the corresponding time point of HG+PM group or the HG+PM group.

results suggest that HG and PM can promote endothelial inflammation and mitophagy by the JNK signaling pathway. NCur reduced this effect.

PM and HG Induced ICAM-1 Expression in ECs Involves miR-221/miR-222 Downregulation, and NCur Reversed These Effects

High expression levels of miR-221/222 have been demonstrated using miRNA expression profiles in ECs, including HUVECs and EA.hy.926 cells.[46] In addition, previous studies have shown that ICAM-1 is a target of miR-221/222, and they are involved in regulating ICAM-1 expression.[35,47] MiR-221 and miR-222 are encoded in tandem on X chromosomes and are highly homologous conserved miRNAs. Based on TargetScan.org (http://www.targetscan.org), miR-221 and miR-222 are complementary to the ICAM-1 3′UTR flanking between 413 and 418. In addition, we found that miR-221 and miR-222 are also complementary to BNIP3 3′UTR flanking between 1832 and 1837 (Figure 6A). Furthermore, we checked whether posttranscriptional regulation by miR-221/222 was necessary for the levels of ICAM-1 and BNIP3 expression in ECs treated with HG+PM and NCur. HG+PM significantly decreased the levels of both miR-221 and miR-222 expression in ECs, while NCur treatment increased the levels of miR-221/222 expression (Figure 6B). To evaluate the effect of miR-221/222 on mitochondrial ROS, mitochondrial functions, and mitophagy, ECs were transfected with miR-221/222 precursors (miR-221/222 mimics) for 24 hr, followed by incubation with HG for 24 hr and exposure to PM for 8 hr. Transfection of cells with miR-221/222 mimics reduced the mitochondrial ROS by MitoSOX Red staining (Figure 6C), reversed the collapse of ΔΨ by JC-1 staining (Figure 6D), increased the ATP production by ATP assay (Figure 6E), and increased the mitochondrial length by MitoTracker staining in HG+PM-treated HUVECs (Figure 6F). Moreover, miR-221/222 mimics decreased the red fluorescence by AO staining (Figure 6G). Transfection of cells with miR-221/222 mimics reduced HG+PM-induced ICAM-1 and BNIP3 expression (Figure 6H). We also found that miR-221/222 mimics reduced the number of monocytes adhering to HG+PM-treated HUVECs (Figure 6I). These results showed that miR-221/222 are involved in HG+PM-induced endothelial inflammation.

NCur Reduced ROS Production, Mitophagy, and Inflammation in the Aortas of PM-Exposed Diabetic Mice

Diabetic mice were established by intraperitoneal injection of STZ and intratracheal injection of PM to mimic mice exposed to air pollution. The PM exposure experimental procedure has been widely used to establish in mouse models and extrapolate air pollution to humans.[48,49] Blood glucose levels were significantly higher in the STZ+PM group than in the STZ or PM alone treatment group. NCur significantly reduced blood glucose levels in STZ-induced diabetic mice exposed to PM (STZ+PM+NCur) compared with the STZ+PM group, indicating that NCur ameliorated hyperglycemia in diabetic mice. (Figure 7A). Furthermore, serum alanine aminotransferase (ALT, as an indicator of liver function) levels were higher in the STZ+PM group than in the STZ or PM groups, and NCur treatment significantly reduced ALT levels compared to the STZ+PM group. The level of creatinine, a marker of renal function, was significantly higher in the STZ group than in the control group and also higher in the STZ+PM group than in the PM group; however, there was no significant difference between the STZ+PM group and the STZ+PM+NCur group. To verify whether NCur affects the ROS production in the aortas of PM-exposed diabetic mice, mitochondrial superoxide anion ($O_2^{\bullet-}$) in the aorta was detected using MitoSOX Red. The results showed increased red fluorescence in the STZ, PM, and STZ+PM groups. Under NCur treatment, red fluorescence was reduced (Figure 7B), suggesting that NCur can inhibit mitochondrial $O_2^{\bullet-}$ production in the m ouse aorta. Moreover, we checked the effects of NCur on inflammation, mitochondrial fission, and autophagy-related and mitophagy-related proteins in diabetic mice exposed to PM by Western blot. The expression levels of ICAM-1, p-DRP1, FIS1, BNIP3, and LC3B were increased in the STZ+PM group. In contrast, NCur treatment significantly decreased the levels of these proteins (Figure 7C), suggesting that NCur attenuated inflammation, mitochondrial fission, autophagy, and mitophagy in the aortas of PM-treated diabetic mice. Furthermore, ICAM-1 and CD31 immunofluorescence revealed that STZ+PM induced aortic endothelial inflammation, whereas NCur treatment attenuated these changes (Figure 7D). Ultrastructural observation of mouse aortic endothelium by transmission electron microscopy (TEM) revealed that mice exposed to STZ+PM had increased autophagosome-like structures in aortic endothelial cells,

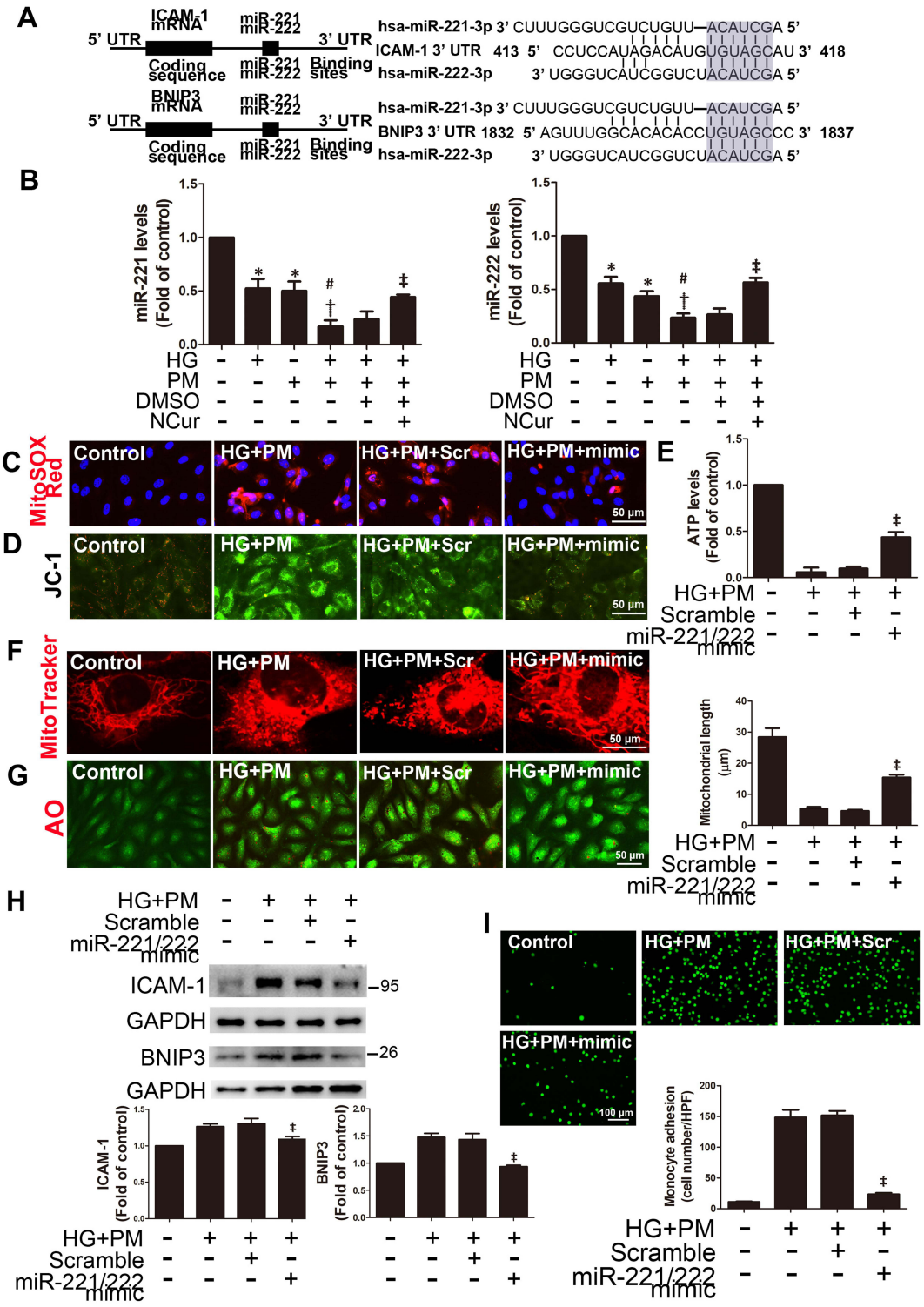

Figure 6 PM and HG-induced inflammation and mitophagy in ECs involves miR-221/miR-222 downregulation, and NCur reversed these effects.

Notes: HUVECs were transfected with miR-221/222 mimics (mimic) or scramble mimic (Scr) for 24 hr, and cells were pretreated with HG (30 mM) for 24 hr and then treated with PM (10 μg/mL) for 8 hr. (**A**) Graphical illustration of miR-221/222 targeting ICAM-1 and BNIP3 3' UTR, respectively. (**B**) The effects of HG, PM, and NCur treatment on miR-221/222 levels in HUVECs. (**C**) The effect of miR-221/222 mimics on mitochondrial ROS in HG+PM-treated HUVECs were detected by MitoSOX Red staining under a fluorescence microscope. Bar=50 μm. (**D**) The effect of miR-221/222 mimics on ΔΨm in HG+PM-treated HUVECs were detected by JC-1 staining under a fluorescence microscope. Bar=50 μm. (**E**) The effect of miR-221/222 mimics on ATP levels in HG+PM-treated HUVECs. (**F**) The effect of miR-221/222 mimics on mitochondrial length in HG+PM-treated HUVECs were determined by MitoTracker staining under a spinning disc confocal microscope. Bar=50 μm. (**G**) The effect of miR-221/222 mimics on the autolysosome formation in HG+PM-treated HUVECs. Bar=50 μm. (**H**) The effects of miR-221/222 mimics on the levels of ICAM-1 and BNIP3 expression in HG+PM-treated HUVECs by Western blot. (**I**) The effects of the transfection of miR-221/222 mimics on fluorescein-labeled THP-1 monocytes adherent to HUVECs. N=5. $^{*}P$ <0.05 compared with the control group; $^{\dagger}P$ <0.05 compared with the HG group; $^{\#}P$ <0.05 compared with the PM group; $^{\ddagger}P$ <0.05 compared with the HG +PM+DMSO group or the HG+PM+Scramble group.

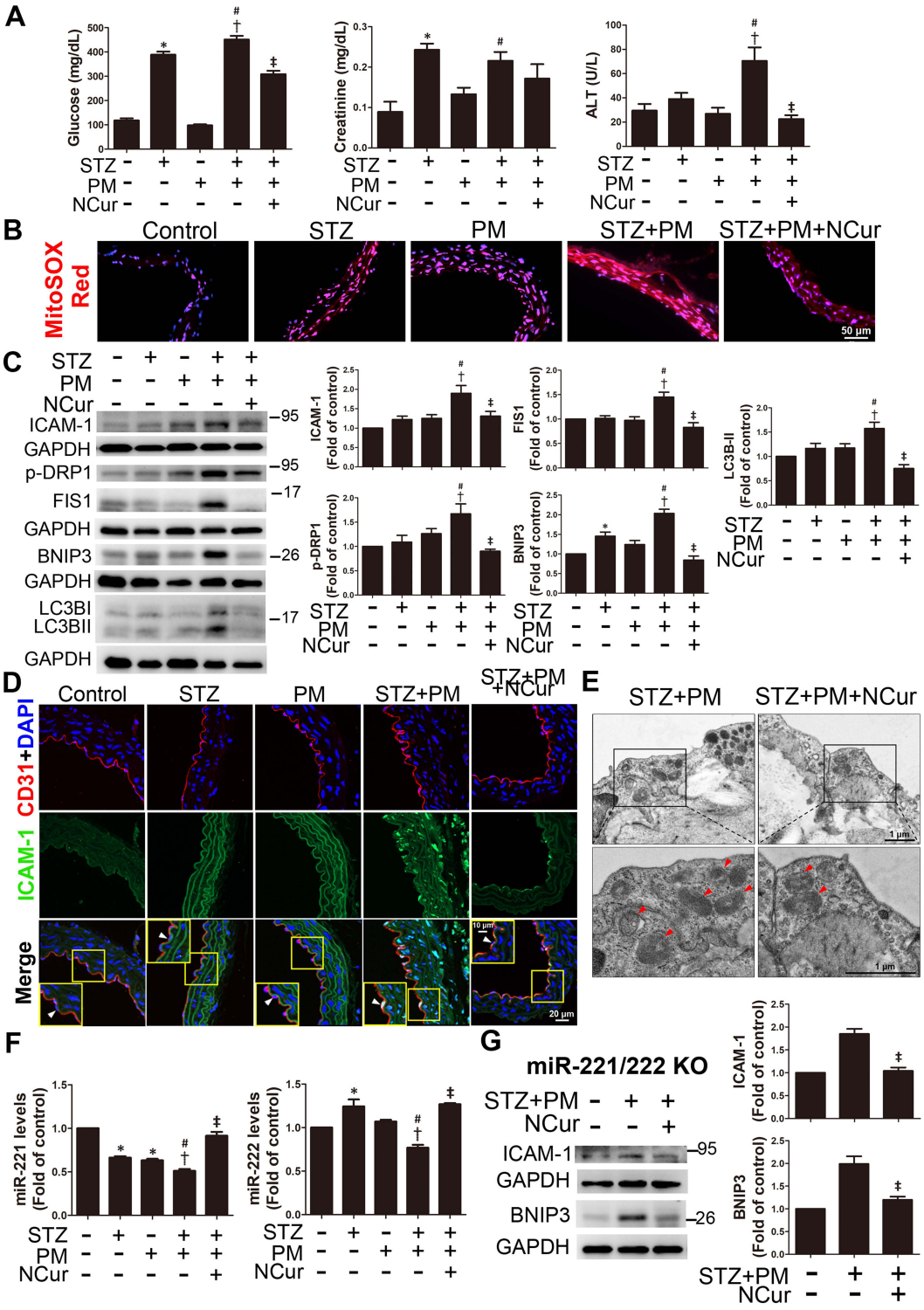

Figure 7 The effects of NCur on mouse aortas under STZ and PM conditions.

Notes: Diabetes was established in mice by intraperitoneal injection of STZ (55 mg/kg) for consecutive five days and overnight fasting. PM (10 mg/kg) was injected intratracheally into mice under anesthesia to simulate air pollution (PM) exposure. NCur was administered orally at a dose of 15 mg/kg once every two days for two weeks. (**A**) The effects of NCur on the levels of blood glucose, creatinine and ALT were analyzed by biochemical kits. (**B**) Oxidative stress levels in cryosections of mouse aorta were detected by MitoSOX Red staining. Red fluorescence in MitoSOX Red-stained sections indicates oxidative stress; blue fluorescence in DAPI-stained sections indicates nuclei. Bar=50 μm. (**C**) The levels of ICAM-1, p-DRP1, FIS1, BNIP3, and LC3B expression were detected using Western blot. (**D**) Immunofluorescence staining indicated the ICAM-1 (green) co-localized with CD31 (red, endothelial cell marker) in STZ+PM-treated aorta. DAPI, blue, nuclear counterstain. White arrows indicated endothelial cells. Bar=25 or 10 μm as the panel indicated. (**E**) Ultrastructure of aortic endothelium examined by TEM. Autophagosomes were indicated by red arrowheads. Bar=1 μm. (**F**) miR-221/222 levels determined by TaqMan qPCR. (**G**) The effects of NCur on the expression of ICAM-1 and BNIP3 in STZ+PM-treated miR-221/222 KO mice were detected by Western blot. $^{*}P$ <0.05 compared with the control group; $^{\dagger}P$ <0.05 compared with the STZ group; $^{\#}P$ <0.05 compared with the PM group; $^{\ddagger}P$ <0.05 compared with the STZ+PM group.

whereas NCur attenuated these changes (Figure 7E). To assess the role of miR-221/222 on aortic endothelial inflammation, we performed miR-221/222 TaqMan qPCR. The levels of miR-221/222 expression were significantly reduced in STZ+PM-treated aortas, while NCur reversed the downregulation of miR-221/222 (Figure 7F). To elucidate the role of miR-221/222 on STZ+PM-induced endothelial inflammation, miR-221/222 KO mice were used in this study. STZ+PM treatment increased the levels of ICAM-1 and BNIP3 expression in miR-221/222 KO mice, whereas NCur decreased the expression (Figure 7G). Based on these results, it was suggested that NCur could protect the aortas of PM-exposed diabetic mice by reducing mitochondrial ROS production, mitochondrial fission, mitophagy, and inflammation. MiR-221/222 plays an important role in endothelial inflammation induced by hyperglycemia and air pollutant, and NCur exerts a protective effect by regulating miR-221/222.

Discussion

The main results of this study demonstrated that concurrent exposure to HG and PM exacerbated endothelial inflammation through increased mitochondrial oxidative stress, mitochondrial fission, and mitophagy. The JNK signaling pathway primarily mediated this process. In addition, miR-221/222 participated in mitophagy and inflammation by specifically targeting BNIP3 and ICAM-1, respectively. Notably, NCur treatment attenuated the detrimental effects of combined exposure to HG and PM. Moreover, PM treatment increased mitochondrial oxidative stress, mitochondrial fission, mitophagy, and inflammation in STZ-induced hyperglycemic mice, while NCur effectively alleviated endothelial injury. NCur demonstrated its antioxidant properties to ameliorate endothelial dysfunction induced by exposure to air pollution under hyperglycemia conditions. These findings highlight the potential therapeutic benefits of NCur in protecting ECs from the adverse effects of air pollution and hyperglycemia.

Air pollution is a concern now and in the future, because it not only worsens diabetes but also promotes the development of CVD.[1] Endothelial inflammation is an important factor in CVD dysfunction,[8] and is associated with HG or PM-induced inflammation in previous reports.[10,50] PM2.5 promotes endothelial inflammation by upregulating ICAM-1 expression.[11,51] Similarly, HG-induced inflammation is mediated through the upregulation of ICAM-1 in ECs.[52,53] Furthermore, previously reported studies showed that HG or PM alone increased ICAM-1 in ECs and promoted monocyte adhesion to ECs.[11,54] Few studies have examined the relationship between PM exposure and the progression of diabetes-induced CVD. A previous study showed that PM2.5-induced metabolic disorders were via activation of NLRP3 inflammasome in diabetic model mice, but not in wild-type mice,[55] which means that inflammation caused by PM and HG plays a role in metabolic diseases. Our recent findings showed that HUVEC treated with 50 μg/mL PM under HG conditions exerted a synergistic effect on endothelial inflammation, which was attenuated by vitamin D treatment.[56] In this study, we further revealed that simultaneous exposure to low doses of PM (10 μg/mL) and HG synergistically affected endothelial inflammation. The detailed mechanisms included mitochondrial fission and the action of miR-221/222, which target BNIP3 and ICAM-1, respectively. Notably, NCur treatment effectively reduced inflammation in this condition.

Cur or NCur has been recognized as a potential treatment for diabetic patients.[57] Previous studies and meta-analyses have highlighted their beneficial effects in reducing CVD risk by improving glycemic and lipid profiles and inflammation.[58] In particular, Cur supplementation has been shown to attenuate PM2.5-induced oxLDL-mediated oxidative stress and inflammation in human microvascular endothelial cells.[59] In addition, NCur has been shown to mitigate STZ-induced pancreatic β cell inflammation and apoptosis and attenuate copper sulfate-induced cardiac injury, oxidative stress, and inflammation.[60,61] Moreover, co-supplementation with omega-3 fatty acids and NCur reduced ICAM-1 gene expression and serum levels in migraineurs.[62] In this study, the effectiveness of NCur in treating endothelial dysfunction following combined exposure to HG and PM was investigated. The results showed that 2 μM NCur treatment significantly increased cell viability and decreased ICAM-1 expression in ECs co-treated with HG and PM, while the same dose of Cur had no such effect. We demonstrated that NCur is more efficient than Cur in sustaining cell viability in HG- and PM-treated ECs. Interestingly, NCur was superior to Cur in promoting insulin levels, antioxidant enzyme activities (SOD, GSH) and PDX1 expression while reducing pancreatic caspase 3 in the STZ-induced diabetic rat model.[63] In the present study, we further demonstrated that NCur significantly suppressed mitochondrial ROS production, mitochondrial fission, mitophagy, and inflammation in ECs exposed to HG and PM. Furthermore,

animal experiments using STZ-induced diabetic mice exposed to PM confirmed the cell-based findings. Such animal models of PM administration have been established and commonly used.[64,65] In this study, NCur treatment reduced mitochondrial ROS, mitochondrial fission, mitophagy, and inflammation in the aortas of PM-treated diabetic mice.

ROS generated by HG treatment alone or exposure to PM alone was associated with endothelial damage.[11,66] Mitochondria control the primary generation of ROS and superoxide is the proximal mitochondrial ROS.[67] In this study, we observed a significant increase in mitochondrial ROS levels after HG and PM treatment. MitoQ or NCur treatment effectively reduced mitochondrial ROS levels in HG+PM-treated ECs. These findings are consistent with previous reports demonstrating the efficacy of NCur in reducing ROS levels in various contexts, such as lowering low-level laser therapy-induced enhancement of ROS in mouse embryonic fibroblasts and decreasing the levels of 8-oxo-2'-deoxyguanosine, which is a sensitive biomarker of ROS-induced DNA damage in an STZ-induced rat model.[60,68] Additionally, the overproduction of mitochondrial ROS can lead to mitochondrial fission when exposed to HG or PM alone,[69,70] and it has been linked to mitophagy and inflammation in acute kidney injury and ischemia-reperfusion-induced acute kidney injury, respectively.[71,72] Previous studies have shown that biomass-derived PM2.5 can induce mitochondrial fission by upregulating p-DRP1 in human airway epithelial cells and airborne PM2.5 induces mitochondrial dysfunction by increasing the mitochondrial fission protein FIS1 in ECs.[14,73] Furthermore, our experiments demonstrated that PM deteriorates mitochondrial membrane potential, reduces ATP production, and increases mitochondrial fission under HG conditions due to the accumulation of mitochondrial ROS.

Autophagy is critical for regulating normal endothelial function.[74] Previous studies have shown that resveratrol and vitamin D protect ECs from inflammation and cell death, respectively, by modulating autophagy.[75,76] Autophagy can be monitored by autophagic flux indicators such as LC3B-II and p62.[77] In this study, we investigated whether PM affects the autophagic events of ECs under HG conditions. Previous reports showed that both PM and HG treatment activates autophagy in ECs.[78,79] Here, we demonstrated that PM aggravates autophagy in HG-treated HUVECs, suggesting that air pollutants further enhance autophagic flux under HG conditions. Furthermore, mitochondrial ROS production results in mitochondrial dysfunction, and these damaged mitochondria are then engulfed by mitochondria-specific macroautophagy, termed mitophagy.[21] BNIP3, a mitophagy-related protein, is related to the induction of mitophagy.[80] Previous studies have linked HG or PM exposure to mitophagy-induced endothelial damage or epithelial damage.[81,82] Our results revealed that PM significantly enhanced autophagy under HG conditions by upregulating autophagy-related proteins LC3B-II and p62, as well as mitophagy-related protein BNIP3. Simultaneous exposure of cells to PM and HG also increased the formation of autophagosome as observed via AO staining. Furthermore, although curcumin has been shown to promote mitophagy in other contexts, such as attenuating osteoarthritis or intestinal barrier damage,[83,84] the role of NCur in mitophagy was previously unknown. This study demonstrated that increases in mitochondrial ROS and inflammation under HG and PM conditions are associated with increased autophagy and mitophagy, as evidenced by upregulation of p62, LC3B, and BNIP3 expression levels. Importantly, NCur treatment reduced these effects, indicating that NCur attenuates HG- and PM-induced mitophagy, thereby alleviating endothelial injury.

The MAPK pathway has been implicated in inflammation or endothelial damage induced by HG or PM alone.[85,86] However, little information is available on the role of MAPK pathways in ECs exposed to both HG and PM. The current study investigated this phenomenon and revealed that the JNK inhibitor SP600125 significantly attenuated the increased ICAM-1 levels after HG and PM treatment, suggesting JNK pathway plays a role in HG and PM-induced endothelial inflammation. In addition, the JNK signaling pathway has been validated to induce defense mechanisms to protect organisms against oxidative or foreign substances by regulating autophagy.[87] Specifically, the JNK pathway is associated with the activation of DUSP1-mediated BNIP3 phosphorylation in ischemia/reperfusion cardiac injury.[88] Another study showed that Mst1 deletion attenuated hyperglycemia-induced vascular dysfunction by reducing mitochondrial fission and regulating JNK signaling.[89] Furthermore, previous reports showed that NCur treatment attenuated cardiac injury in copper sulfate-intoxicated rats through MAPK pathway and reduced bisphenol A-induced cardiotoxicity through p38 and JNK pathway.[61,90]

Differentially expressed microRNAs under pathological or physiological stress have been associated with CVD.[31,91,92] Our previous research showed that exosomes carrying miR-221/222 from adipose-derived stem cells protected against cardiac damage induced by ischemia/reperfusion.[93] In addition, miR-221/222 have been shown to

regulate ICAM-1 expression in TNF-α-induced inflammation in lung epithelial and ECs, respectively, in our previous reports.[34,35] Studies have demonstrated that miR-221/222 play crucial roles in regulating lipid metabolism, inflammation, fibrosis in the liver, and improving inflammation in viral myocarditis.[32,94] Moreover, miR-221/222 promotes insulin intolerance by inhibiting insulin production by pancreatic β cells in mice.[95] These findings make them a significant player in the development of diabetes. In this study, HG and PM treatment decreased the miR-221/222 levels in ECs. However, NCur treatment reversed this decrease. A previous report showed that miRNAs are the novel targets of curcumin in cancer therapy.[96] In addition, curcumin is related to the transcriptional activation of microRNA such as miR-21 through AP-1 (activator protein-1).[97] Moreover, curcumin has been shown to selectively inhibit NF-κB, a regulator of miR-21, thereby reducing its expression.[98,99] Therefore, NCur may regulate miR-221/222 expression through transcriptional regulation or by modulating miR-221/222 degradation via RNase.[100] In this study, cells transfected with miR-221/222 mimics exhibited reduced ROS production and autophagosomes induced by HG and PM. Moreover, these cells displayed improved ΔΨm and mitochondrial length. Furthermore, cells transfected with miR-221/222 mimics reduced ICAM and BNIP3 expression and inhibited monocyte adhesion. These findings suggest that NCur increases the expression of miR-221/222, thereby mitigating ICAM-1-mediated endothelial inflammation.

In this study, NCur has been shown to be effective as a therapeutic agent in ameliorating HG- and PM-induced endothelial inflammation. Its protective role involves the regulation of miR-221/222 and the clearance of mitochondrial ROS. However, the underlying mechanism by which NCur upregulates miR-221/222 remains unclear. Previous studies have suggested that Cur affects miRNA regulation in cancer therapy,[96] and plays a key role in miRNA transcription and post-transcriptional degradation.[98,100] Therefore, NCur may exert the above-mentioned effects by promoting the expression of miR-221/222, and the specific mechanism deserves further study. Furthermore, it's worth noting that the PM doses used in in vivo studies are widely used in toxicological testing.[64] However, limitations of this study regarding these doses may extend beyond real-world exposures. These issues require further investigation to elucidate the molecular mechanism of NCur and to fully understand the actual effect of PM on organisms.

Conclusion

In this study, the combined exposure to PM and HG exacerbated mitochondrial oxidative stress and mitochondrial fission, mitophagy, and inflammation in ECs. The JNK pathway played a pivotal role in these processes. However, NCur pretreatment effectively attenuated endothelial injury both in vitro and in vivo. These findings highlight the potential of NCur as a therapeutic intervention to counteract the detrimental effects of simultaneous exposure to diabetes and air pollutants on endothelial cells. This research provides the importance of investigating new approaches, such as NCur, to protect people with diabetes from the adverse effects of environmental pollutants, raising hope for improved strategies to manage diabetes-related cardiovascular complications exacerbated by air pollution.

Abbreviations

ΔΨm, mitochondrial membrane potential; CVD, cardiovascular disease; ECs, endothelial cells; HG, high glucose; HUVECs, human umbilical vein endothelial cells; KO, knockout; miR, microRNA; NCur, nanocurcumin; NO, nitric oxide; PM, particulate matter; ROS, reactive oxygen species; STZ, streptozotocin.

Data Sharing Statement

Data analyzed during the current study are available from the corresponding author upon request.

Ethics Approval

All animal experiments were conducted in accordance with the Guidelines for Animal Care of National Taiwan University (IACUC approval no: 20180426) and in accordance with the Guidelines for the Care and Use of Laboratory Animals (NIH publication no. 86–23, revised in 1985).

Acknowledgments

We thank the technical services provided by the "Transgenic Mouse Models Core Facility of the National Core Facility for Biopharmaceuticals, National Science and Technology Council, Taiwan" and the "Gene Knockout Mouse Core Laboratory of National Taiwan University Center of Genomic and Precision Medicine". In addition, we thank the imaging core and flow cytometric analyzing and sorting core of the first core laboratory, National Taiwan University College of Medicine, for the technical support in image acquisition and analysis.

Author Contributions

All authors made a significant contribution to the work reported, whether that is in the conception, study design, execution, acquisition of data, analysis and interpretation, or in all these areas; took part in drafting, revising or critically reviewing the article; gave final approval of the version to be published; have agreed on the journal to which the article has been submitted; and agree to be accountable for all aspects of the work.

Funding

This work was supported by research grants from the National Science and Technology Council (MOST 108-2320-B-002-065-MY3; MOST 111-2320-B-002-022-MY3 to Y.L.C, and NSTC 112-2320-B-005-003- to T.C.L), the National Taiwan University Hospital (111-S0169; 112S0182 to J.S.T), and Partially supported by the iECG and Animal Biotechnology Center from the Feature Areas Research Center Program within the framework of the Higher Education Sprout Project by the Ministry of Education (MOE-111-S-0023-A) in Taiwan (T.C.L), and Chang Gung University of Science Foundation (Grant No. ZRRPF6M0011 to C.W.L).

Disclosure

Authors declare that they have no competing interests.

References

1. Al-Kindi SG, Brook RD, Biswal S, Rajagopalan S. Environmental determinants of cardiovascular disease: lessons learned from air pollution. *Nat Rev Cardiol*. 2020;17(10):656–672. doi:10.1038/s41569-020-0371-2
2. Pope CA, Turner MC, Burnett RT, et al. Relationships between fine particulate air pollution, cardiometabolic disorders, and cardiovascular mortality. *Circ Res*. 2015;116(1):108–115. doi:10.1161/circresaha.116.305060
3. Wang M, Zhou T, Song Y, et al. Joint exposure to various ambient air pollutants and incident heart failure: a prospective analysis in UK Biobank. *Eur Heart J*. 2021;42(16):1582–1591. doi:10.1093/eurheartj/ehaa1031
4. Dal Canto E, Ceriello A, Rydén L, et al. Diabetes as a cardiovascular risk factor: an overview of global trends of macro and micro vascular complications. *Eur J Prev Cardiol*. 2019;26(2_suppl):25–32. doi:10.1177/2047487319878371
5. Thiering E, Heinrich J. Epidemiology of air pollution and diabetes. *Trends Endocrinol Metab*. 2015;26(7):384–394. doi:10.1016/j.tem.2015.05.002
6. Su PF, Sie FC, Yang CT, Mau YL, Kuo S, Ou HT. Association of ambient air pollution with cardiovascular disease risks in people with type 2 diabetes: a Bayesian spatial survival analysis. *Environ Health*. 2020;19(1):110. doi:10.1186/s12940-020-00664-0
7. O'Neill MS, Veves A, Zanobetti A, et al. Diabetes enhances vulnerability to particulate air pollution–associated impairment in vascular reactivity and endothelial function. *Circulation*. 2005;111(22):2913–2920. doi:10.1161/circulationaha.104.517110
8. Lv Y, Kim K, Sheng Y, et al. YAP controls endothelial activation and vascular inflammation through TRAF6. *Circ Res*. 2018;123(1):43–56. doi:10.1161/circresaha.118.313143
9. Hou W, Lu L, Li X, Sun M, Zhu M, Miao C. c-Myc participates in high glucose-mediated endothelial inflammation via upregulation of IRAK1 expression in diabetic nephropathy. *Cell Signal*. 2022;92:110263. doi:10.1016/j.cellsig.2022.110263
10. Pope CA, Bhatnagar A, McCracken JP, Abplanalp W, Conklin DJ, O'Toole T. Exposure to fine particulate air pollution is associated with endothelial injury and systemic inflammation. *Circ Res*. 2016;119(11):1204–1214. doi:10.1161/circresaha.116.309279
11. Rui W, Guan L, Zhang F, Zhang W, Ding W. PM2.5-induced oxidative stress increases adhesion molecules expression in human endothelial cells through the ERK/AKT/NF-κB-dependent pathway. *J Appl Toxicol*. 2016;36(1):48–59. doi:10.1002/jat.3143
12. Chen F, Ma D, Li A. SENP3 regulates high glucose-induced endothelial dysfunction via ROS dependent signaling. *Diab Vasc Dis Res*. 2020;17(6):1479164120970895. doi:10.1177/1479164120970895
13. Liu H, Xiang H, Zhao S, et al. Vildagliptin improves high glucose-induced endothelial mitochondrial dysfunction via inhibiting mitochondrial fission. *J Cell Mol Med*. 2019;23(2):798–810. doi:10.1111/jcmm.13975
14. Miao X, Li W, Niu B, et al. Mitochondrial dysfunction in endothelial cells induced by airborne fine particulate matter (<2.5 μm). *J Appl Toxicol*. 2019;39(10):1424–1432. doi:10.1002/jat.3828
15. Xia WR, Fu W, Wang Q, et al. Autophagy induced FHL2 upregulation promotes IL-6 production by activating the NF-κB pathway in mouse aortic endothelial cells after exposure to PM2.5. *Int J Mol Sci*. 2017;18(7):1484. doi:10.3390/ijms18071484

16. Fan W, Han D, Sun Z, et al. Endothelial deletion of mTORC1 protects against hindlimb ischemia in diabetic mice via activation of autophagy, attenuation of oxidative stress and alleviation of inflammation. *Free Radic Biol Med*. 2017;108:725–740. doi:10.1016/j.freeradbiomed.2017.05.001
17. Lim CC, Hayes RB, Ahn J, et al. Mediterranean diet and the association between air pollution and cardiovascular disease mortality risk. *Circulation*. 2019;139(15):1766–1775. doi:10.1161/circulationaha.118.035742
18. Li D, Yang S, Xing Y, et al. Novel insights and current evidence for mechanisms of atherosclerosis: mitochondrial dynamics as a potential therapeutic target. *Front Cell Dev Biol*. 2021;9:673839. doi:10.3389/fcell.2021.673839
19. Mizushima N, Levine B, Cuervo AM, Klionsky DJ. Autophagy fights disease through cellular self-digestion. *Nature*. 2008;451(7182):1069–1075. doi:10.1038/nature06639
20. Choi AM, Ryter SW, Levine B. Autophagy in human health and disease. *N Engl J Med*. 2013;368(7):651–662. doi:10.1056/NEJMra1205406
21. Palikaras K, Lionaki E, Tavernarakis N. Mechanisms of mitophagy in cellular homeostasis, physiology and pathology. *Nat Cell Biol*. 2018;20(9):1013–1022. doi:10.1038/s41556-018-0176-2
22. Bravo-San Pedro JM, Kroemer G, Galluzzi L. Autophagy and mitophagy in cardiovascular disease. *Circ Res*. 2017;120(11):1812–1824. doi:10.1161/circresaha.117.311082
23. Ning R, Li Y, Du Z, et al. The mitochondria-targeted antioxidant MitoQ attenuated PM(2.5)-induced vascular fibrosis via regulating mitophagy. *Redox Biol*. 2021;46:102113. doi:10.1016/j.redox.2021.102113
24. Xiang J, Zhang C, Di T, et al. Salvianolic acid B alleviates diabetic endothelial and mitochondrial dysfunction by down-regulating apoptosis and mitophagy of endothelial cells. *Bioengineered*. 2022;13(2):3486–3502. doi:10.1080/21655979.2022.2026552
25. Mitchell PS, Parkin RK, Kroh EM, et al. Circulating microRNAs as stable blood-based markers for cancer detection. *Proc Natl Acad Sci U S A*. 2008;105(30):10513–10518. doi:10.1073/pnas.0804549105
26. Ueda T, Volinia S, Okumura H, et al. Relation between microRNA expression and progression and prognosis of gastric cancer: a microRNA expression analysis. *Lancet Oncol*. 2010;11(2):136–146. doi:10.1016/s1470-2045(09)70343-2
27. Karolina DS, Tavintharan S, Armugam A, et al. Circulating miRNA profiles in patients with metabolic syndrome. *J Clin Endocrinol Metab*. 2012;97(12):E2271–E2276. doi:10.1210/jc.2012-1996
28. Devaux Y, Vausort M, Goretti E, et al. Use of circulating microRNAs to diagnose acute myocardial infarction. *Clin Chem*. 2012;58(3):559–567. doi:10.1373/clinchem.2011.173823
29. Tang R, Long T, Lui KO, Chen Y, Huang ZP. A roadmap for fixing the heart: RNA regulatory networks in cardiac disease. *Mol Ther Nucleic Acids*. 2020;20:673–686. doi:10.1016/j.omtn.2020.04.007
30. Wang C, Wang S, Zhao P, et al. MiR-221 promotes cardiac hypertrophy in vitro through the modulation of p27 expression. *J Cell Biochem*. 2012;113(6):2040–2046. doi:10.1002/jcb.24075
31. Liu X, Xiao J, Zhu H, et al. miR-222 is necessary for exercise-induced cardiac growth and protects against pathological cardiac remodeling. *Cell Metab*. 2015;21(4):584–595. doi:10.1016/j.cmet.2015.02.014
32. Corsten MF, Heggermont W, Papageorgiou AP, et al. The microRNA-221/-222 cluster balances the antiviral and inflammatory response in viral myocarditis. *Eur Heart J*. 2015;36(42):2909–2919. doi:10.1093/eurheartj/ehv321
33. Tian Z, Miyata K, Kadomatsu T, et al. ANGPTL2 activity in cardiac pathologies accelerates heart failure by perturbing cardiac function and energy metabolism. *Nat Commun*. 2016;7:13016. doi:10.1038/ncomms13016
34. Liu CW, Sung HC, Lin SR, et al. Resveratrol attenuates ICAM-1 expression and monocyte adhesiveness to TNF-α-treated endothelial cells: evidence for an anti-inflammatory cascade mediated by the miR-221/222/AMPK/p38/NF-κB pathway. *Sci Rep*. 2017;7:44689. doi:10.1038/srep44689
35. Sung HC, Liu CW, Hsiao CY, et al. The effects of wild bitter gourd fruit extracts on ICAM-1 expression in pulmonary epithelial cells of C57BL/6J mice and microRNA-221/222 knockout mice: involvement of the miR-221/-222/PI3K/AKT/NF-κB pathway. *Phytomedicine*. 2018;42:90–99. doi:10.1016/j.phymed.2018.03.023
36. Hettiarachchi SS, Dunuweera SP, Dunuweera AN, Rajapakse RMG. Synthesis of curcumin nanoparticles from raw turmeric rhizome. *ACS Omega*. 2021;6(12):8246–8252. doi:10.1021/acsomega.0c06314
37. Afifi M, Alkaladi A, Abomughaid MM, Abdelazim AM. Nanocurcumin improved glucose metabolism in streptozotocin-induced diabetic rats: a comparison study with Gliclazide. *Environ Sci Pollut Res Int*. 2020;27(20):25271–25277. doi:10.1007/s11356-020-08941-8
38. Quispe C, Herrera-Bravo J, Javed Z, et al. Therapeutic applications of curcumin in diabetes: a review and perspective. *Biomed Res Int*. 2022;2022:1375892. doi:10.1155/2022/1375892
39. Schantz MM, Cleveland D, Heckert NA, et al. Development of two fine particulate matter standard reference materials (< 4 µm and< 10 µm) for the determination of organic and inorganic constituents. *Anal Bioanal Chem*. 2016;408(16):4257–4266. doi:10.1007/s00216-016-9519-7
40. Chattopadhyay K, Samanta A, Mukhopadhyay S, Chattopadhyay B. Potential amelioration of nicotine-induced toxicity by nanocurcumin. *Drug Dev. Res.* 2018;79(3):119–128. doi:10.1002/ddr.21424
41. Pu CM, Liu CW, Liang CJ, et al. Adipose-derived stem cells protect skin flaps against ischemia/reperfusion injury via IL-6 expression. *J Investig Dermatol*. 2017;137(6):1353–1362. doi:10.1016/j.jid.2016.12.030
42. Forrester SJ, Kikuchi DS, Hernandes MS, Xu Q, Griendling KK. Reactive oxygen species in metabolic and inflammatory signaling. *Circ Res*. 2018;122(6):877–902. doi:10.1161/circresaha.117.311401
43. Westermann B. Mitochondrial fusion and fission in cell life and death. *Nat Rev Mol Cell Biol*. 2010;11(12):872–884. doi:10.1038/nrm3013
44. Lin Q, Li S, Jiang N, et al. PINK1-parkin pathway of mitophagy protects against contrast-induced acute kidney injury via decreasing mitochondrial ROS and NLRP3 inflammasome activation. *Redox Biol*. 2019;26:101254. doi:10.1016/j.redox.2019.101254
45. Mauvezin C, Neufeld TP. Bafilomycin A1 disrupts autophagic flux by inhibiting both V-ATPase-dependent acidification and Ca-P60A/SERCA-dependent autophagosome-lysosome fusion. *Autophagy*. 2015;11(8):1437–1438. doi:10.1080/15548627.2015.1066957
46. Suárez Y, Fernández-Hernando C, Pober JS, Sessa WC. Dicer dependent microRNAs regulate gene expression and functions in human endothelial cells. *Circ Res*. 2007;100(8):1164–1173. doi:10.1161/01.Res.0000265065.26744.17
47. Duan M, Yao H, Hu G, Chen X, Lund AK, Buch S. HIV Tat induces expression of ICAM-1 in HUVECs: implications for miR-221/-222 in HIV-associated cardiomyopathy. *PLoS One*. 2013;8(3):e60170. doi:10.1371/journal.pone.0060170

48. Li X, Yang H, Sun H, et al. Taurine ameliorates particulate matter-induced emphysema by switching on mitochondrial NADH dehydrogenase genes. *Proc Natl Acad Sci U S A*. 2017;114(45):E9655–E9664. doi:10.1073/pnas.1712465114
49. Wang Y, Liao S, Pan Z, et al. Hydrogen sulfide alleviates particulate matter-induced emphysema and airway inflammation by suppressing ferroptosis. *Free Radic Biol Med*. 2022;186:1–16. doi:10.1016/j.freeradbiomed.2022.04.014
50. Shen X, Chen X, Wang J, et al. SET8 suppression mediates high glucose-induced vascular endothelial inflammation via the upregulation of PTEN. *Exp Mol Med*. 2020;52(10):1715–1729. doi:10.1038/s12276-020-00509-3
51. Zou L, Xiong L, Wu T, et al. NADPH oxidases regulate endothelial inflammatory injury induced by PM(2.5) via AKT/eNOS/NO axis. *J Appl Toxicol*. 2022;42(5):738–749. doi:10.1002/jat.4254
52. Kim SW, Kim CE, Kim MH. Flavonoids inhibit high glucose-induced up-regulation of ICAM-1 via the p38 MAPK pathway in human vein endothelial cells. *Biochem Biophys Res Commun*. 2011;415(4):602–607. doi:10.1016/j.bbrc.2011.10.115
53. Li B, Li H, Dai L, et al. NIK-SIX1 signalling axis regulates high glucose-induced endothelial cell dysfunction and inflammation. *Autoimmunity*. 2022;55(2):86–94. doi:10.1080/08916934.2021.2015579
54. Liu R, Shen H, Wang T, et al. TRAF6 mediates high glucose-induced endothelial dysfunction. *Exp Cell Res*. 2018;370(2):490–497. doi:10.1016/j.yexcr.2018.07.014
55. Song L, Lei L, Jiang S, et al. NLRP3 inflammasome is involved in ambient PM(2.5)-related metabolic disorders in diabetic model mice but not in wild-type mice. *Inhal Toxicol*. 2021;33(6–8):260–267. doi:10.1080/08958378.2021.1980637
56. Lai TC, Chen YC, Cheng HH, et al. Combined exposure to fine particulate matter and high glucose aggravates endothelial damage by increasing inflammation and mitophagy: the involvement of vitamin D. *Part Fibre Toxicol*. 2022;19(1):25. doi:10.1186/s12989-022-00462-1
57. Marton LT, Pescinini ESLM, Camargo MEC, et al. The Effects of curcumin on diabetes mellitus: a systematic review. *Front Endocrinol*. 2021;12:669448. doi:10.3389/fendo.2021.669448
58. Ashtary-Larky D, Rezaei Kelishadi M, Bagheri R, et al. The Effects of nano-curcumin supplementation on risk factors for cardiovascular disease: a GRADE-assessed systematic review and meta-analysis of clinical trials. *Antioxidants*. 2021;10(7). doi:10.3390/antiox10071015
59. Shi J, Deng H, Zhang M. Curcumin pretreatment protects against PM2.5-induced oxidized low-density lipoprotein-mediated oxidative stress and inflammation in human microvascular endothelial cells. *Mol Med Rep*. 2017;16(3):2588–2594. doi:10.3892/mmr.2017.6935
60. Ganugula R, Arora M, Jaisamut P, et al. Nano-curcumin safely prevents streptozotocin-induced inflammation and apoptosis in pancreatic beta cells for effective management of Type 1 diabetes mellitus. *Br J Pharmacol*. 2017;174(13):2074–2084. doi:10.1111/bph.13816
61. Sarawi WS, Alhusaini AM, Fadda LM, et al. Nano-curcumin prevents cardiac injury, oxidative stress and inflammation, and modulates TLR4/NF-κB and MAPK signaling in copper sulfate-intoxicated rats. *Antioxidants*. 2021;10(9). doi:10.3390/antiox10091414
62. Soveyd N, Abdolahi M, Djalali M, et al. The combined effects of ω −3 fatty acids and nano-curcumin supplementation on intercellular adhesion molecule-1 (ICAM-1) gene expression and serum levels in migraine patients. *CNS Neurol Disorders Drug Targets*. 2018;16(10):1120–1126. doi:10.2174/1871527317666171213154749
63. Metawea MR, Abdelrazek HMA, El-Hak HNG, Moghazee MM, Marie OM. Comparative effects of curcumin versus nano-curcumin on histological, immunohistochemical expression, histomorphometric, and biochemical changes to pancreatic beta cells and lipid profile of streptozocin induced diabetes in male Sprague-Dawley rats. *Environ Sci Pollut Res Int*. 2023. doi:10.1007/s11356-023-26260-6
64. Driscoll KE, Costa DL, Hatch G, et al. Intratracheal instillation as an exposure technique for the evaluation of respiratory tract toxicity: uses and limitations. *Toxicol Sci*. 2000;55(1):24–35. doi:10.1093/toxsci/55.1.24
65. Zhang Y, Liu M, Fan R, et al. Walnut protein isolates attenuate particulate matter-induced lung and cardiac injury in mice and zebra fish. *RSC Adv*. 2019;9(69):40736–40744. doi:10.1039/c9ra06002b
66. Lin F, Yang Y, Wei S, et al. Hydrogen sulfide protects against high glucose-induced human umbilical vein endothelial cell injury through activating PI3K/Akt/eNOS pathway. *Drug Des Devel Ther*. 2020;14:621–633. doi:10.2147/dddt.S242521
67. Murphy MP. How mitochondria produce reactive oxygen species. *Biochem J*. 2009;417(1):1–13. doi:10.1042/bj20081386
68. Ebrahiminaseri A, Sadeghizadeh M, Moshaii A, Asgaritarghi G, Safari Z. Combination treatment of dendrosomal nanocurcumin and low-level laser therapy develops proliferation and migration of mouse embryonic fibroblasts and alter TGF-β, VEGF, TNF-α and IL-6 expressions involved in wound healing process. *PLoS One*. 2021;16(5):e0247098. doi:10.1371/journal.pone.0247098
69. Liu X, Zhao X, Li X, et al. PM(2.5) triggered apoptosis in lung epithelial cells through the mitochondrial apoptotic way mediated by a ROS-DRP1-mitochondrial fission axis. *J Hazard Mater*. 2020;397:122608. doi:10.1016/j.jhazmat.2020.122608
70. Abuarab N, Munsey TS, Jiang LH, Li J, Sivaprasadarao A. High glucose-induced ROS activates TRPM2 to trigger lysosomal membrane permeabilization and Zn(2+)-mediated mitochondrial fission. *Sci Signal*. 2017;10(490). doi:10.1126/scisignal.aal4161
71. Su L, Zhang J, Gomez H, Kellum JA, Peng Z. Mitochondria ROS and mitophagy in acute kidney injury. *Autophagy*. 2023;19(2):401–414. doi:10.1080/15548627.2022.2084862
72. Zhao M, Wang Y, Li L, et al. Mitochondrial ROS promote mitochondrial dysfunction and inflammation in ischemic acute kidney injury by disrupting TFAM-mediated mtDNA maintenance. *Theranostics*. 2021;11(4):1845–1863. doi:10.7150/thno.50905
73. Gao M, Liang C, Hong W, et al. Biomass-related PM2.5 induces mitochondrial fragmentation and dysfunction in human airway epithelial cells. *Environ. Pollut.* 2022;292(Pt B):118464. doi:10.1016/j.envpol.2021.118464
74. Nussenzweig SC, Verma S, Finkel T. The role of autophagy in vascular biology. *Circ Res*. 2015;116(3):480–488. doi:10.1161/circresaha.116.303805
75. Chen ML, Yi L, Jin X, et al. Resveratrol attenuates vascular endothelial inflammation by inducing autophagy through the cAMP signaling pathway. *Autophagy*. 2013;9(12):2033–2045. doi:10.4161/auto.26336
76. Uberti F, Lattuada D, Morsanuto V, et al. Vitamin D protects human endothelial cells from oxidative stress through the autophagic and survival pathways. *J Clin Endocrinol Metab*. 2014;99(4):1367–1374. doi:10.1210/jc.2013-2103
77. Yoshii SR, Mizushima N. Monitoring and measuring autophagy. *Int J Mol Sci*. 2017;18(9). doi:10.3390/ijms18091865
78. Wang Y, Tang M. PM2.5 induces autophagy and apoptosis through endoplasmic reticulum stress in human endothelial cells. *Sci Total Environ*. 2020;710:136397. doi:10.1016/j.scitotenv.2019.136397
79. Zhao X, Su L, He X, Zhao B, Miao J. Long noncoding RNA CA7-4 promotes autophagy and apoptosis via sponging MIR877-3P and MIR5680 in high glucose-induced vascular endothelial cells. *Autophagy*. 2020;16(1):70–85. doi:10.1080/15548627.2019.1598750

80. Zhang J, Ney PA. Role of BNIP3 and NIX in cell death, autophagy, and mitophagy. *Cell Death Differ*. 2009;16(7):939–946. doi:10.1038/cdd.2009.16
81. Zhang Y, Wang S, Chen X, et al. Liraglutide prevents high glucose induced HUVECs dysfunction via inhibition of PINK1/Parkin-dependent mitophagy. *Mol Cell Endocrinol*. 2022;545:111560. doi:10.1016/j.mce.2022.111560
82. Mizumura K, Justice MJ, Schweitzer KS, et al. Sphingolipid regulation of lung epithelial cell mitophagy and necroptosis during cigarette smoke exposure. *FASEB j*. 2018;32(4):1880–1890. doi:10.1096/fj.201700571R
83. Cao S, Wang C, Yan J, Li X, Wen J, Hu C. Curcumin ameliorates oxidative stress-induced intestinal barrier injury and mitochondrial damage by promoting Parkin dependent mitophagy through AMPK-TFEB signal pathway. *Free Radic Biol Med*. 2020;147:8–22. doi:10.1016/j.freeradbiomed.2019.12.004
84. Jin Z, Chang B, Wei Y, et al. Curcumin exerts chondroprotective effects against osteoarthritis by promoting AMPK/PINK1/Parkin-mediated mitophagy. *Biomed Pharmacother*. 2022;151:113092. doi:10.1016/j.biopha.2022.113092
85. Wang Y, Xiong L, Wu T, et al. Analysis of differentially changed gene expression in EA.hy926 human endothelial cell after exposure of fine particulate matter on the basis of microarray profile. *Ecotoxicol Environ Saf*. 2018;159:213–220. doi:10.1016/j.ecoenv.2018.05.002
86. Fei Y, Sun L, Yuan C, Jiang M, Lou Q, Xu Y. CFTR ameliorates high glucose-induced oxidative stress and inflammation by mediating the NF-κB and MAPK signaling pathways in endothelial cells. *Int J Mol Med*. 2018;41(6):3501–3508. doi:10.3892/ijmm.2018.3547
87. Zhou YY, Li Y, Jiang WQ, Zhou LF. MAPK/JNK signalling: a potential autophagy regulation pathway. *Biosci Rep*. 2015;35(3):e00199. doi:10.1042/BSR20140141
88. Jin Q, Li R, Hu N, et al. DUSP1 alleviates cardiac ischemia/reperfusion injury by suppressing the Mff-required mitochondrial fission and Bnip3-related mitophagy via the JNK pathways. *Redox Biol*. 2018;14:576–587. doi:10.1016/j.redox.2017.11.004
89. Qin R, Lin D, Zhang L, Xiao F, Guo L. Mst1 deletion reduces hyperglycemia-mediated vascular dysfunction via attenuating mitochondrial fission and modulating the JNK signaling pathway. *J Cell Physiol*. 2020;235(1):294–303. doi:10.1002/jcp.28969
90. Valokola MG, Karimi G, Razavi BM, et al. The protective activity of nanomicelle curcumin in bisphenol A-induced cardiotoxicity following subacute exposure in rats. *Environ Toxicol*. 2019;34(3):319–329. doi:10.1002/tox.22687
91. Rao PK, Toyama Y, Chiang HR, et al. Loss of cardiac microRNA-mediated regulation leads to dilated cardiomyopathy and heart failure. *Circ Res*. 2009;105(6):585–594. doi:10.1161/circresaha.109.200451
92. Sayed D, Hong C, Chen IY, Lypowy J, Abdellatif M. MicroRNAs play an essential role in the development of cardiac hypertrophy. *Circ Res*. 2007;100(3):416–424. doi:10.1161/01.Res.0000257913.42552.23
93. Lai TC, Lee TL, Chang YC, et al. MicroRNA-221/222 Mediates ADSC-exosome-induced cardioprotection against ischemia/reperfusion by targeting PUMA and ETS-1. *Front Cell Dev Biol*. 2020;8:569150. doi:10.3389/fcell.2020.569150
94. Di Martino MT, Arbitrio M, Caracciolo D, et al. miR-221/222 as biomarkers and targets for therapeutic intervention on cancer and other diseases: a systematic review. *Mol Ther Nucleic Acids*. 2022;27:1191–1224. doi:10.1016/j.omtn.2022.02.005
95. Fan L, Shan A, Su Y, et al. MiR-221/222 inhibit insulin production of pancreatic β-cells in mice. *Endocrinology*. 2020;161(1):bqz027. doi:10.1210/endocr/bqz027
96. Mirzaei H, Masoudifar A, Sahebkar A, et al. MicroRNA: a novel target of curcumin in cancer therapy. *J Cell Physiol*. 2018;233(4):3004–3015. doi:10.1002/jcp.26055
97. Mudduluru G, George-William JN, Muppala S, et al. Curcumin regulates miR-21 expression and inhibits invasion and metastasis in colorectal cancer. *Biosci Rep*. 2011;31(3):185–197. doi:10.1042/bsr20100065
98. Yang CH, Yue J, Fan M, Pfeffer LM. IFN induces miR-21 through a signal transducer and activator of transcription 3-dependent pathway as a suppressive negative feedback on IFN-induced apoptosis. *Cancer Res*. 2010;70(20):8108–8116. doi:10.1158/0008-5472.Can-10-2579
99. Yang CH, Yue J, Sims M, Pfeffer LM. The curcumin analog EF24 targets NF-κB and miRNA-21, and has potent anticancer activity in vitro and in vivo. *PLoS One*. 2013;8(8):e71130. doi:10.1371/journal.pone.0071130
100. Zhang Z, Qin YW, Brewer G, Jing Q. MicroRNA degradation and turnover: regulating the regulators. *Wiley Interdiscip Rev RNA*. 2012;3(4):593–600. doi:10.1002/wrna.1114